DEVELOPMENT OF NEW THREE-DIMENSIONAL ROCK MASS STRENGTH CRITERIA

Mohammad Hadi Mehranpour[1,2], Pinnaduwa H S W Kulatilake[1*], Ma Xingen[3] and Manchao He[3]

[1]Rock Mass Modeling and Computational Rock Mechanics Laboratories, University of Arizona, Tucson, AZ, 85721, USA

[2]Now at HPT-laboratory, Faculty of Geosciences, Utrecht University, Utrecht, Netherlands

[3]State Key Laboratory for Geomechanics and Deep Underground Engineering, China University of Mining and Technology Beijing, China

*Corresponding author: kulatila@u.arizona.edu

Abstract

Two new three-dimensional rock mass strength criteria are developed in this paper by extending an existing rock mass strength criterion. These criteria incorporate the effects of the intermediate principal stress, minimum principal stress and the anisotropy resulting from these stresses acting on the fracture system. In addition, these criteria have the capability of capturing the anisotropic and scale dependent behavior of the jointed rock mass strength by incorporating the effect of fracture geometry through the fracture tensor components. The new criteria are proposed after analyzing 284 numerical modeling results of the polyaxial, triaxial and biaxial compression tests conducted on the jointed rock blocks having one or two joint sets by the PFC^{3D} software. Some of these simulation results were compared with experimental results to validate the developed PFC^{3D} model that was used for numerical modeling of jointed blocks. In this research to have several samples with the same properties a synthetic rock material that is made out of a mixture of gypsum, sand and water was used. Altogether, 12 joint systems were chosen; some of them had one joint set and the rest had two joint sets. Joint sets have different dip angles varying from 15° to 45° at an interval of 15° with dip directions of 30° and 75° for the two joint sets. Each joint set also has 3 persistent joints with the joint spacing of 42 mm in a cubic sample of size 160 mm. The minimum and intermediate principal stress combination

values were chosen based on the uniaxial compressive strength (UCS) value of the modeled intact synthetic rock. The minimum principal stress values were chosen as 0, 0.2, 0.4 and 0.6 of the UCS. For each minimum principal stress value, the intermediate principal stress value varies starting at the minimum principal stress value and increasing at an interval of 0.2 of the UCS until it is slightly lower than the strength of the sample under the biaxial loading condition with the same minimum principal stress value. To express the new rock mass strength criteria, it was also necessary to determine the intact rock strengths under the same confining stress combinations mentioned earlier. Therefore, the intact rock was also modeled for all three compression tests and the intact rock strengths were found for 33 different minimum and intermediate principal stress combinations.

Keywords

Discrete Element Method (DEM), Particle Flow Code (PFC), Rock mass strength, Polyaxial compression test, Intermediate principal stress, Fracture Tensor

List of Symbols

A	Disk area
a, a_2, a_3, b, b_2, b_3	Empirical coefficients
B	An empirical constant
B^J	Constant coefficient of the Modified Smooth-Joint Contact model
C_J	Joint cohesion
D_{min}, D_{max}	Minimum and maximum particle diameters
E_c, $\bar{E}_c$	Contact and bond Young's modulus of the Linear Parallel Bond Model, respectively
F_{ij}, F_{ij}^r, F_{ij}^k	Fracture tensor, Fracture tensor of the rock mass and Fracture tensor of the k^{th} joint set, respectively

F_{11}, F_{22}, F_{33}	Fracture tensor components in the maximum, intermediate and minimum principal stress directions, respectively
f, f_2, f_3	monotonically decreasing functions
K_n^J, K_s^J	Joint normal and shear stiffnesses, respectively
k_n^J, k_s^J	Joint normal and shear stiffnesses of the Modified Smooth-Joint Contact model, respectively
$k_{n_{min}}^J$	Minimum joint normal stiffness of the Modified Smooth-Joint Contact model
k_r, $\bar{k}_r$	Ratio of the normal to shear stiffnesses of the contact and bond for the Linear Parallel Bond Model, respectively
m	Number of parameters to be estimated
$m^{(V)}$	Number of fracture centers
N	Total number of joint sets
n	Total number of data sets
$\boldsymbol{n}$	Normal vector
n_i, n_j	Projection of the normal vector in the directions of $\boldsymbol{i}$ and $\boldsymbol{j}$, respectively
p, p_2, p_3, q, q_2, q_3	Empirical coefficients
R^2	Coefficient of determination
r	Equivalent radius
S_r	Strength ratio between the jointed rock mass and intact rock strengths
V	Assumed volume
X, Y, Z	Cartesian coordinates
λ, λ_0, λ_2, λ_3	Empirical coefficients
$\bar{\lambda}$	Bond radius fraction of the Linear Parallel Bond Model

μ	Friction coefficient of the Linear Parallel Bond Model
μ^J	Joint friction coefficient of the Modified Smooth-Joint Contact model
$\sigma_1, \sigma_2, \sigma_3$	Maximum, Intermediate and Minimum principal stresses, respectively
σ_c	Uniaxial compressive strength
$\bar{\sigma}_c, \bar{\tau}_s$	Bond tensile and shear strengths of the Linear Parallel Bond Model, respectively
σ_J, σ_I	Jointed rock mass and intact rock strengths, respectively
$\sigma_{J,i}^P$	Predicted jointed rock block strength from the new rock mass strength criterion for data set *i*
$\sigma_{J,i}^{PFC}$	Strength of the jointed rock block from the PFC^{3D} modeling for data set *i*
$\bar{\sigma}_J^{PFC}$	Average strength value of all the PFC^{3D} data
σ_n	Normal stress
σ_n^J	Normal stress on the Modified Smooth-Joint Contact
φ_J	Joint friction angle

Abbreviations

CUMTB	China University of Mining and Technology, Beijing
DEM	Discrete Element Method
JSC	Joint Sides Checking approach
LPBM	Linear Parallel Bond Model
LVDT	Linear Variable Differential Transformer
MSJCM	Modified Smooth-Joint Contact model
NIOSH	National Institute for Occupational Safety and Health

PFC	Particle Flow Code
PFC^{3D}	Three-dimensional Particle Flow Code
SJCM	Smooth-Joint Contact Model
UCS	Uniaxial Compressive Strength
3DEC	Three-dimensional Distinct Element Code

1. Introduction

Jointed rock masses are known as the combination of intact rock blocks and discontinuities. Therefore, the mechanical behavior of a rock mass is affected by the mechanical behavior of intact rock and discontinuities in addition to the discontinuity geometry. The number of discontinuity sets, their intensity, spatial distribution of orientation, size and spacing, roughness, strength and deformation of asperities, filling, aperture, are the important properties of rock discontinuities which can affect the mechanical behavior of rock masses. Thus, assessment of the mechanical behavior of a jointed rock mass is relatively more complicated compared to that of an intact rock due to the high number of parameters that affect the mechanical behavior of rock masses (Kulatilake 1985; Yu 2001). On the other hand, unfortunately, understanding of the mechanical behavior of rock masses is crucial to design safe and economical structures in or on jointed rock masses.

Moreover, due to the presence of complicated discontinuity geometry patterns, the inherent statistical nature of discontinuity geometrical parameters, and the variabilities and uncertainties involved in the estimation of discontinuity mechanical and geometrical properties, estimation of the mechanical behavior of discontinuous rock masses is difficult and challenging (Kulatilake 1985; Kulatilake et al. 1993).

Analytical, Empirical, and numerical are three available approaches to estimate mechanical behavior of rock masses (Kulatilake et al. 1993; Goel and Singh 2011; Kulatilake 2016). Analytical approaches provide analytical solutions for rock mass strength criteria based on selecting suitable intact rock and rock joint strength criteria and applying simplified methods to combine them. This method is rarely applicable in dealing with field rock masses, which are usually more complicated than the assumed simplified models (Bekaert and Maghous 1996; Pouya and Ghoreychi 2001).

On the other hand, the empirical approach based on one of the rock mass classification systems is simple and it may be used in complicated conditions to obtain some preliminary estimates of rock mass mechanical properties. However, in all rock mass classification systems, personal judgment, and experience play crucial roles (Bieniawski 1973; Barton et al. 1974; Hoek 1994). Moreover, in the rock mass classification systems, the isotropic behavior is assumed for the rock masses. However, most rock masses show anisotropic behavior due to the existence of distinct orientations of discontinuity sets (Kulatilake et al. 1993; Amadei 1996; Marinos et al. 2005; Wu and Kulatilake 2012; Chiu et al. 2013). Therefore, the available rock mass strength criteria based on the rock mass classification systems are unable to capture the anisotropic behavior of rock masses as well as the effect of the intermediate principal stress on the rock mass strength. It should be mentioned that even though some researchers (Pan and Hudson 1988; Priest 2005; Melkoumian et al. 2009; Zhang and Zhu 2007; Zhang 2008; Zhang et al. 2013; Saroglou and Tsiambaos 2008; Colak and Unlu 2004; Ismael et al. 2014; Yudhbir et al. 1983; Sheorey et al. 1989) tried to incorporate the effect of the intermediate principal stress in their formulations to overcome one of the above-mentioned shortcomings, their proposed criteria have not captured the effect of joint orientation and scale (resulting from joint size) on rock mass strength explicitly.

Ramamurthy (2001) instead of using the rock mass classification systems to quantify the effect of rock joint systems, proposed a joint factor parameter which is related to the joint frequency and the joint orientation. However, it does not consider the complete effect of joint orientation on rock mass strength resulting from multiple joint sets. In addition, this criterion does not consider the scale effect and the effect of the intermediate principal stress on the rock mass strength.

Nowadays through accessibility to extremely fast computers, numerical modeling can be used as an approach to overcome the shortcomings of the analytical and empirical approaches by incorporating the mechanical behavior of intact rocks and rock joints to find the mechanical behavior of rock masses (Kulatilake et al. 1993; Wu and Kulatilake 2012; Shreedharan and Kulatilake 2016). Moreover, the new methods like digital photogrammetry and LiDAR can help to extract the geometrical properties of rock discontinuities with high resolution leading to better accuracy of numerical modeling results (Gigli and Casagli 2011; Zheng et al. 2014; Kulatilake and Shu 2015). Numerical modeling can be used to estimate rock mass strength by incorporating fracture geometry and using constitutive models for the intact rock and rock joint behavior.

For jointed rock mass strength evaluation, in addition to the above-mentioned parameters, the boundary and environmental conditions such as the in-situ stress, loading/unloading stress path, loading rate, pore pressure, temperature, humidity etc. are important factors to consider (Goel and Singh 2011). Thus, numerical modeling is very useful because of its power to apply different boundary conditions on the models. Polyaxial (or true-triaxial) boundary stress condition is one the most important conditions which can be considered in numerical modeling. In the polyaxial stress condition, three principal stresses (maximum principal stress, σ_1, intermediate principal stress, σ_2, minimum principal stress, σ_3,) are not equal ($\sigma_1 < \sigma_2 < \sigma_3$) (Mehranpour and Kulatilake 2016). Although the polyaxial stress is a common condition in the real field situation which has a significant effect on the jointed rock mass strength, it has been considered rarely in the rock mechanics literature and the effect of the intermediate principal stress is generally ignored. Mehranpour and Kulatilake (2017) clearly showed the effect of the intermediate principal stress on the strength of jointed rock by extending Jaeger's theory and numerical modeling with the Particle Flow Code (PFC) approach, which belongs to the Discrete Element Method (DEM) category.

Because several parameters affect the strength of rock masses, numerous experimental tests are required to find the effect of these parameters on the strength of rock masses. That task is time consuming, very costly and impractical to perform in the field and laboratory. To solve this problem some researchers modeled rock masses with numerical modeling to propose new rock mass failure criteria. In this method, at first, a numerical model is calibrated with a limited number of experimental tests and physical modeling of the rock masses and then the calibrated model is expanded to more complicated situations with more diverse conditions (Kulatilake et al. 1993; Pouya and Ghoreychi 2001; Kulatilake et al. 2001 and 2006; Wu and Kulatilake 2012a; He et al. 2016). Kulatilake et al. (1993) and Wu and Kulatilake (2012) used this procedure incorporating the 3DEC software, which is one of the well-known DEM software packages used in the rock mechanics field, to find the effect of the joint geometry parameters on the deformability properties of rock masses. To quantify the joint geometry parameters, they used an extended form of the fracture tensor concept. Kulatilake et al. (2001and 2006) and He et al. (2016) also extended the fracture tensor concept to fracture tensor components and developed new rock mass strength criteria.

In this paper, the same procedure is used based on experimental tests and PFC^{3D} modeling on intact rock, jointed rock with one joint set and jointed rock with two non-orthogonal joint sets to develop new rock mass strength criteria in three dimensions. The new criteria consider the effect of all principal stresses in three dimensions and they are applicable for any type of rock mass, especially for non-sedimentary rock masses which generally have non-

orthogonal fracture systems. This criterion also shows the anisotropic strength behavior of rock masses due to the dip angle and dip direction of joint sets. It should be mentioned that compared to other numerical methods, in the PFC, macro parameter values are not directly used in the numerical model, and micro parameter values applicable between the particles should be calibrated using the macro property values, and then these calibrated micro parameter values are used in PFC modeling.

To develop new rock mass strength criteria, first conventional experimental tests on the intact rock and the joint as well as the polyaxial compression tests on the intact rock and jointed samples are performed on the synthetic rock samples. Then the micro properties of PFC^{3D} model are calibrated based on the experimental test results. Afterwards, polyaxial, triaxial and biaxial compression tests for the intact rock and jointed rock blocks are simulated in the PFC^{3D} with different combinations of minimum and intermediate principal stresses. After gathering results, the development of new rock mass failure criteria was initiated using the fracture tensor concept which was introduced by Oda (1982) and developed into the fracture tensor components by Kulatilake et al. (1993, 2006). Fracture tensor combines the joint orientation, joint size, joint density for each joint set and the number of joint sets by a second order tensor. Thus, the fracture tensor can show the anisotropy and scale effects of rock masses which are exhibited by the presence of joints.

It should be mentioned that polyaxial and triaxial compression tests were performed in the laboratory with a limited number of boundary stress conditions and joint set systems, because the experimental tests are expensive, and the apparatus had limited load capacity. Then, these experimental tests were simulated using PFC^{3D} and the numerical results were compared with the experimental results of synthetic intact rock and synthetic jointed rock blocks. If these two groups of results did not match, micro parameter values were modified until very close results were obtained with an acceptable error. According to these steps, estimation of appropriate values for micro mechanical properties was done; it turned out to be one of the challenging parts of this project. All the above-mentioned procedures used to develop new rock mass strength criteria are shown in the flowchart given in Fig. 1.

2. Laboratory tests

As mentioned in the introduction, new rock mass strength criteria were developed based on the computational results obtained from the calibrated and validated PFC^{3D} model. Note that the macro mechanical experimental results obtained for the synthetic intact rock and synthetic rock joints were used for the calibration of the PFC^{3D} model.

Besides, a limited number of polyaxial and triaxial compression tests were also performed on the synthetic intact rock and synthetic jointed rock samples to compare with the numerical modeling results to validate the calibrated PFC^{3D} model. In this validation procedure, it was necessary to modify the micro mechanical property values if the numerical and experimental results were not similar.

2.1. Sample preparation

For the experimental part, to have several samples with the same properties, a synthetic material that was made of a mixture of gypsum, sand and water was used. This model material exhibits different mechanical properties depending on the mixture ratio. This ratio was designed to have the samples based on the loading limitation of the loading machine which was used in the laboratory. The experimental tests were performed at the China University of Mining and Technology, Beijing (CUMTB) based on the test preparation and loading conditions designed by the Rock Mass Modeling and Computational Rock Mechanics Laboratories at the University of Arizona. The water to gypsum ratio of each sample was 0.6:1 by weight. After casting the gypsum samples in the mold, samples were kept in the room temperature (20±2°C) for one day. Then, samples were placed in a humidity chamber which can control temperature and humidity at different levels. Samples were kept in a humidity chamber for a week with the temperature set to 20±2°C and the relative humidity set to 100%. Finally, samples were taken out from the humidity chamber and were kept in the room temperature (20±2°C) until they were used for experimental tests.

2.2 Intact rock experimental tests

In the first step of the experimental program, 3 uniaxial tests, 3 triaxial tests and 5 Brazilian tests were performed on the synthetic intact rock material. Thus, from these tests, macro mechanical parameter values of the Young's modulus, uniaxial compressive strength (UCS), internal friction angle, cohesion and Poisson's ratio for the synthetic intact rock were obtained and the summary results are given in Table 1. These macro mechanical property values were used to calibrate the micro properties of the synthetic intact rock. Uniaxial and triaxial compression tests were performed on cubic samples of side dimension 160 mm. The polyaxial compression test facility available at the CUMTB (Fig. 2) was used to apply forces on all sides of the cubical samples. This machine has the capability to apply a maximum force of 500 KN on each of the three perpendicular directions (two horizontal directions and the vertical direction) with 0.5% accuracy. Applied load was measured in each of the perpendicular directions. Two LVDT deformation sensors were used to measure the deformation in each of the perpendicular directions. The deformation

range for each direction is 150 mm with 0.4% accuracy. Loading, data collection and saving were done automatically through a data acquisition and a computer system. Fig. 3 shows the uniaxial and triaxial test results obtained from the polyaxial compression test facility. These test results were used to calibrate and validate the built PFC^{3D} model for the synthetic intact rock.

2.3 Rock joint experimental tests

In addition to estimating the macro mechanical properties of the synthetic intact rock, it was necessary to estimate the macro mechanical properties of the synthetic rock joint to calibrate the micro mechanical properties for joints. The joint friction angle, φ_J, joint cohesion, C_J, joint normal stiffness, K_n^J, and the joint shear stiffness, K_s^J, are important mechanical properties of the synthetic rock joint. Several researchers realized that the joint normal stiffness varies with the normal stress acting on the joint surfaces and they have proposed different relations to describe this behavior (Shehata 1972; Goodman 1976; Bandis et al. 1983; Swan 1983; Malama and Kulatilake 2003; Kulatilake et al. 2016). Kulatilake et al. (2016) developed the linear relation given by equation 1 between the joint normal stiffness and the normal stress acting on the joint plane, σ_n, and showed that it has a good correlation with experimental test results obtained by the same research group.

$$K_n^J = B\sigma_n \quad (1)$$

In equation 1, B is an empirical constant. Thus, instead of finding the joint normal stiffness the B value should be found. In this research, 3 direct shear tests and 4 joint normal stiffness tests were performed on the synthetic rock joint to estimate the macro mechanical properties of the joint and the estimated values are given in Table 2. Fig. 4 shows the detailed experimental test results obtained from the direct shear tests and joint normal stiffness tests. For the direct shear tests and joint normal stiffness tests cylindrical samples with 50 mm diameter and the heights of 50 mm and 100 mm were used, respectively.

2.4 Polyaxial and triaxial compression tests

Polyaxial and triaxial compression tests were performed on a limited number of intact rock and jointed rock samples with one joint set to verify the numerical modeling performed on the polyaxial and triaxial compression tests with the calibrated PFC^{3D} model. The same polyaxial testing machine explained in Section 2.2 was used to perform the polyaxial and triaxial compression tests on the cubic synthetic intact rock and synthetic jointed rock samples with

255 the dimension of 160 mm. In the polyaxial test, first the minimum principal stress was applied on the sample in all
256 three perpendicular directions. Then the stress on one lateral direction was kept constant ($= \sigma_3$) and the stress equal
257 to the intermediate principal stress was applied in the other two directions. Finally, the stress in the second lateral
258 direction was kept constant ($= \sigma_2$) and the axial stress in the vertical direction was increased until the sample failed.

259 The jointed rock samples had 3 joints with the joint spacing of 42 mm, the dip direction of 30° and the dip angles of
260 15° or 30° for the different samples. Figs. 5 and 6 show the schematic diagrams of these jointed samples as well as
261 the prepared samples for experimental tests. Due to the importance of the directions of the applied principal stresses
262 on the jointed samples for their polyaxial compression test, the same direction was used for each principal stress. For
263 the jointed rock block samples, the maximum principal stress was applied vertically, and the other two principal
264 stresses were applied horizontally where the angles between the intermediate and minimum principal stress directions
265 and the joint dip direction were 30° and 60°, respectively (Figs. 5 and 6). Table 3 and Figs. 7-9 show the applied σ_2
266 and σ_3 stresses and the results of the above-mentioned experimental polyaxial and triaxial compression tests. Table 3
267 shows that for the same minimum principal stress, the strength of the intact rock and jointed rock increases with
268 increasing intermediate principal stress. Besides, this table shows a strength reduction as the dip angle of the joint set
269 increases from 15° to 30°under the same confining stresses.

270 **3. Numerical modeling**

271 For numerical modeling, the PFC approach was chosen. The PFC is a DEM based software, which uses disks
272 (in 2-D) or spherical elements (in 3-D) to represent particles. In this method, particles are assumed as rigid and
273 Newton's second law controls the interactions between the particles. Particles can have contact with adjacent particles
274 and force-displacement law acts at contacts (Cundall and Strack 1979; Cundall and Hart 1992). The PFC can
275 conveniently model the fracture initiation and propagation between the particles, as well as the rupture, using the
276 Bonded-Particle Models that cement particles together in representing the intact rock (Potyondy and Cundall 2004;
277 Potyondy 2015). Moreover, in the PFC software to model the mechanical behavior of jointed rock masses the intact
278 rock can be modeled by the Bonded-Particle Models, and the discontinuities can be modeled by the Smooth-Joint
279 Contact Model (SJCM) (Pierce et al. 2007). Therefore, the block breakage as well as joint sliding can be
280 accommodated (Mas Ivars et al. 2011).

As stated before, in the PFC, micro parameter values applicable between the particles should be calibrated using the macro properties. Due to the presence of a higher number of micro mechanical parameters compared to the available macro properties and complex behavior of the micro mechanical parameters, the calibration of micro parameters is based on a trial and error procedure in which the micro mechanical parameter values are varied iteratively to match the macro mechanical behaviors. Therefore, the calibration is one of the most critical and challenging parts in modeling with the PFC. Several researchers such as Kulatilake et al. (2001), Potyondy and Cundall (2004), Cho et al. (2007), Yang et al. (2015) and Mehranpour and Kulatilake (2016) have dealt with this calibration and have indicated their findings on relations between the micro and macro parameters. Several others have used the PFC in modeling intact rocks or jointed rock masses (Fakhimi 2004; Koyama and Jing 2007; Park and Song 2009; Lee and Jeon 2011; Schöpfer et al. 2013; Zhang et al. 2015; Fan et al. 2015; Duan and Kwok 2016). However, limited efforts (Yang et al. 2015; Bahaaddini et al. 2015; Mehranpour and Kulatilake 2017) have been made on the calibration and modeling of the joints with the SJCM.

In this research to model the intact rock in PFC^{3D}, among the different Bonded Particle Models, the Linear Parallel Bond Model (LPBM) was chosen for contacts. The LPBM works like a cement material and assumes the two adjacent particles are cemented to each other with a notional rectangular (2D) or cylindrical (3D) shape of contact. The major problem of LPBM is its inability to model the failure envelop for the whole spectrum of rock types. It can only model rocks with the low internal friction angles, and the low ratios of compressive to tensile strength. To solve this problem some researchers have proposed different methods and different models (Potyondy and Cundall 2004; Fakhimi 2004; Cho et al. 2007). The synthetic material which is used in this study has a low internal friction angle and a low ratio of compressive to tensile strength. Thus, the LPBM can model the used synthetic intact rock properly.

For the synthetic intact rock calibration process a cubic sample of side dimension of 160 mm with a uniform particle size distribution (the minimum particle diameter of 2.7 mm and the maximum particle diameter of 4.48 mm) was created in PFC^{3D} to model the uniaxial and triaxial tests mentioned in Section 2.2. Based on the selected particle size distribution, 103,663 particles and 275,824 contacts were produced in the cubic samples of side dimension of 160 mm. For the Linear Parallel Bond Model used for the synthetic intact rock, it is necessary to calibrate the micro mechanical parameters of contact Young's modulus, E_c, bond Young's modulus, $\bar{E}_c$, contact friction coefficient, μ, bond tensile strength, $\bar{\sigma}_c$, bond shear strength, $\bar{\tau}_s$, the ratio of normal to shear stiffness for contact, k_r, ratio of normal to shear stiffness for bond, $\bar{k}_r$ and bond radius fraction, $\bar{\lambda}$, using macro properties of the uniaxial compressive strength,

internal friction angle, Young's modulus, tensile strength and Poisson's ratio. Because the number of micro mechanical parameters is higher than the number of macro mechanical parameters, the assumptions of $E_c = \bar{E}_c, k_r = \bar{k}_r, \bar{\sigma}_c = \bar{\tau}_s$ and $\bar{\lambda} = 1$ were used as recommended by Potyondy and Cundall (2004) and Itasca (2016) to reduce the calibration process difficulty. As stated before, the calibration is a trial and error procedure. Therefore, to minimize the number of iterations in the calibration process the following sequence was followed based on the relations between micro and macro mechanical properties and the guidelines given by Yang et al. (2015) and Mehranpour and Kulatilake (2016). First, in the uniaxial compression test modeling the Young's modulus was calibrated by setting the material strengths to a large value and varying E_c and $\bar{E}_c$ to match the Young's modulus. Next, by changing k_r and $\bar{k}_r$, the Poisson's ratio was matched. After calibrating the above-mentioned micro mechanical parameters, the peak strength was matched by gradually reducing the normal and shear bond strengths of the parallel bonds. Finally, by gradual reduction of μ in modeling of the triaxial compression tests, the internal friction angle was matched. The calibrated micro parameter values are given in Table 4 for Linear Parallel Bond Model. Table 1 shows the obtained macro mechanical parameter values based on PFC^{3D} simulations as well as from laboratory tests. Comparison of the two sets of values indicates the accuracy and capability of the particle flow approach in simulating the synthetic intact rock.

To model the synthetic rock joint in PFC^{3D}, the Modified Smooth-Joint Contact model (MSJCM) was used. The MSJCM was proposed by Mehranpour and Kulatilake (2017) to overcome the shortcoming of the Smooth Joint Contact Model (SJCM) to capture the non-linear behavior of the joint closure varying with the joint normal stress. The MSJCM uses the linear relation between the joint normal stiffness and the normal contact stress given in equation 1 to model the non-linear relation between the joint normal deformation and the joint normal stress observed in the compression joint normal stiffness test. Thus, in the MSJCM instead of assigning a constant value to the joint normal stiffness, k_n^J, a variable value is assigned which is proportional to the normal stress on the smooth-joint contact, σ_n^J, according to the following equation.

$$k_n^J = \max(k_{n_{min}}^J, B^J \sigma_n^J) \quad (2)$$

In equation 2, $k_{n_{min}}^J$ is the minimum value for k_n^J, and B^J is a constant coefficient. It should be mentioned that $k_{n_{min}}^J$ is included since it is impossible to have a zero value for stiffness in PFC. Note that the other micro mechanical parameters for the MSJCM like joint shear stiffness, k_s^J, and joint friction coefficient, μ^J, are the same as for the SJCM.

Mehranpour and Kulatilake (2017) also proposed a new joint contact implementation algorithm in PFC which is called the Joint Sides Checking (JSC) approach to solve the interlocking problem. The interlocking problem was observed by Bahaaddini et al. (2013) and it occurs due to the shortcoming of the updating procedure in the PFC software for the contact conditions of the particles that lie around the intended joint plane during high shear displacements. The interlocking problem leads to higher values for shear strength and dilation angle for the joint than the correct values. It also creates unwanted fractures around the intended joint plane. In this paper the JSC approach is used not only for the calibration procedure of the rock joint model but also for the modeling of the polyaxial, triaxial and biaxial compression tests on the synthetic jointed rock block samples.

In calibrating the joint micro mechanical parameters, first the cylindrical synthetic rock samples with 50 mm diameter, and the heights of 50 mm and 100 mm were numerically modeled based on the Linear Parallel Bond Model properties given in Table 4, for the direct shear tests and the joint normal stiffness test, respectively. Then the MSJCM joint was added horizontally to each sample at the mid-height level with the JSC approach. Then, to calibrate the MSJCM the following sequence was used to minimize the number of iterations. First, all the micro mechanical parameters for MSJCM were set with low values. Then, $k_{n_{min}}^{J}$ and B^{J} were calibrated using the joint normal stiffness test modeling because k_s^J and μ^J values do not affect this test results. In the calibration of joint normal stiffness test, first the B^J value was gradually increased to match the curvature of the normal stress-joint normal displacement diagram and then by increasing the $k_{n_{min}}^{J}$, the total joint normal displacement was matched (see Fig.4a). After $k_{n_{min}}^{J}$ and B^J calibration, in the direct shear test modeling, first k_s^J was gradually increased to match K_s^J and finally, the μ^J value was changed to match the φ_J value (see Fig. 4b). Table 5 shows the calibrated micro mechanical property values of the MSJCM using the JSC approach based on the experimental test results reported for the synthetic rock joint in Section 2.3. Table 2 shows the obtained macro mechanical parameter values based on the PFC^{3D} simulations. Note that Table 2 also provides the macro mechanical parameter values obtained through experimental joint testing. Table 2 along with Figure 4 indicate the accuracy and capability of the PFC in simulating the synthetic rock joint through comparison of PFC^{3D} results against the laboratory test results on synthetic rock joints. For further details about the JSC approach, MSJCM and the interlocking problem the reader is referred to Mehranpour and Kulatilake (2017).

3.1. Polyaxial compression tests

In the performed numerical modeling, three different test types were simulated on the synthetic intact rock and synthetic jointed rock blocks using PFC^{3D} to obtain data to develop suitable rock mass strength criteria. In these simulations like the experimental tests, cubic samples of side dimension 160 mm were used with micro mechanical property values given in Tables 4 and 5. The first test type conducted was the triaxial test ($\sigma_1 > \sigma_2 = \sigma_3$). In simulating this test, the hydraulic stress equal to the minimum principal stress was applied on the sample until the sample reached the equilibrium (1st step in Fig. 10a). Then the stresses on the lateral faces were kept constant ($= \sigma_2 = \sigma_3$) and the axial stress was increased until the sample failed (2nd step in Fig. 10a). The second type of test simulated was the polyaxial (true-triaxial) test ($\sigma_1 > \sigma_2 > \sigma_3$). In this test like in the conventional triaxial test, the hydraulic stress equal to the minimum principal stress was applied on the sample until the sample reached the equilibrium (1st step in Fig. 10b). Then the stress on one lateral direction was kept constant ($= \sigma_3$) and the stress equal to the intermediate principal stress was applied in the other two directions until the sample reached the equilibrium (2nd step in Fig. 10b). Finally, the stress in the second lateral direction was kept constant ($= \sigma_2$) and the axial stress in the vertical direction was increased until the sample failed (3rd step in Fig. 10b). The third test type simulated was the biaxial test ($\sigma_1 = \sigma_2 > \sigma_3$). In this test like in the two previous tests, the hydraulic stress equal to the minimum principal stress was applied on the sample until the sample reached the equilibrium (1st step in Fig. 10c). Then the stress on one lateral direction was kept constant ($= \sigma_3$) and the stresses in the other two directions were increased until the sample failed (2nd step in Fig. 10c).

The minimum and intermediate principal stress combination values of different compression tests were chosen based on the UCS value of the modeled synthetic intact rock. The minimum principal stress values were chosen as 0, 20, 40 and 60 percent of the UCS. For each minimum principal stress value, the intermediate principal stress value varied starting at the minimum principal stress value and increasing at an interval of 20 percent of the UCS until it was slightly lower than the strength of the sample under the biaxial loading condition with the same minimum principal stress value. With this procedure, the applied minimum and intermediate principal stress combinations for samples were the same. Thus, the effect of joint geometry configurations on the rock mass strength can be evaluated properly. Moreover, because the strength of the synthetic intact rock is available for each minimum and intermediate principal stress combination, the normalized strength of jointed rock blocks can be obtained to propose a general rock mass strength criterion.

For jointed rock blocks, twelve different joint systems with one and two joint sets were chosen to cover different types of non-orthogonal fracture systems. Joint sets have different dip angles varying from 15° to 45° at an interval of 15° with dip directions of 30° and 75°. Each joint set has 3 joints with the joint spacing of 42 mm in a cubic sample of size 160 mm. Fig. 11 shows the PFC^{3D} models and the schematic pictures of joint geometry diagrams for all 12 jointed rock blocks. It should be mentioned that for each cubic sample, the minimum principal stress was applied on the faces with the dip directions of 90° and 270° and the intermediate principal stress was applied on the faces with the dip directions of 0° and 180°. It should be mentioned that because the numerical models based on the micro parameter values given in Tables 4 and 5 could reasonably accurately model the experimental test results up to the sample failure (Figs. 7-9), it was not necessary to modify the micro parameter values given in Tables 4 and 5. For each rock joint system under each confining stress combination it took about 2 days on the average to complete an above-mentioned numerical simulation. However, this time duration was smaller for models with lower confining stresses and joint systems with lower dip angles compared to that having higher confining stresses and higher dip angles.

Figs. 12-15 show the rock block strength values obtained for the synthetic jointed and intact rock models under different minimum and intermediate principal stress combinations. Fig 12 shows the rock strength values obtained for the synthetic jointed rock models with 1 joint set compared to the strength of the synthetic intact rock model and Figs. 13-15 show the rock strength values obtained for the synthetic jointed rock models with 2 joint sets under different minimum and intermediate principal stress combinations compared to the strength of the synthetic jointed rock models having 1 joint set with the same properties as the first joint set of the rock sample with 2 joint sets. These figures indicate that for each combination of the minimum and intermediate principal stresses, the jointed rock blocks with 2 joint sets and 1 joint set have resulted in a lower strength compared to that of the synthetic intact rock and the jointed rock blocks with 2 joint sets have resulted in a lower strength value compared to that of the jointed rock blocks having 1 joint set with the same properties as the first joint set of the rock sample with 2 joint sets. This means that adding of joint sets to a sample under the same minimum and intermediate principal stress combination reduces the strength of the sample.

Fig. 12 also shows that the intermediate principal stress has a significant effect on the synthetic intact rock strength and it can increase the intact rock strength up to about 25%. Increase of the intermediate principal stress while

keeping the minimum principal stress constant, increases the strength of intact rock to a peak value and then the strength decreases. However, in Figs. 12-15 for each σ_3 level in the jointed rock models, the reduction of the strength after reaching the peak strength due to increase of σ_2 seems to be lower compared to that of the intact rock model. In some plots, even the strength reduction does not seem to exist especially for low σ_3 values and high joint set dip angles.

4. Development of new rock mass strength criteria

This paper develops new rock mass strength criteria based on the PFC^{3D} modeling results incorporating the fracture tensor concept. The fracture tensor is explained comprehensively in references (Oda 1982; Oda 1984; Kulatilake et al. 1993; Wu and Kulatilake 2012a). In the fracture tensor, it is assumed that each fracture to be a very thin disk having an area A with an equivalent radius of r ($A = \pi r^2$) and two normal vectors of $\boldsymbol{n}$ and $-\boldsymbol{n}$ (bold italic letter represent a vector) for each side of the disk. To find the fracture tensor components of the modeled jointed rock blocks the following equations are used.

$$F_{ij}^{r} = \sum_{k=1}^{N} F_{ij}^{k} \tag{3}$$

$$F_{ij} = \frac{1}{V} \sum^{m^{(V)}} 2\pi r^3 n_i n_j \tag{4}$$

where F_{ij}^{r} is the fracture tensor of the rock mass, F_{ij}^{k} is the fracture tensor (F_{ij}) of the k^{th} joint set, N is the total number of joint sets, $m^{(V)}$ is the number of fracture centers inside the assumed volume of V, and n_i and n_j are the projection of $\boldsymbol{n}$ on the directions of $\boldsymbol{i}$ and $\boldsymbol{j}$, respectively. Table 6 shows the computed fracture tensor components for all 12 different joint systems with one or two joint sets which are modeled using the PFC^{3D}. In this table because the maximum, intermediate and minimum principal stresses are applied in Z, Y and X directions respectively, the alternate subscripts are also used to show the directions of the fracture tensor components with respect to the principal stresses.

Kulatilake et al. (2006) showed that for the biaxial loading in the laboratory on about 150 synthetic rock blocks having two joint sets with 30 different joint systems in which the joint set dip directions were towards the intermediate principal stress direction, the rock mass strength, σ_J, under a constant intermediate principal stress, reduces non-linearly with increasing fracture tensor component in the intermediate principal stress direction (F_{22}). After trying various functions such as hyperbolic, negative power and negative exponential functions they proposed the following negative exponential equation which had the best regression fit to the experimental test results:

$$\frac{\sigma_J}{\sigma_I} = e^{-\lambda F_{22}} \quad (5)$$

In equation 5, σ_I is the intact rock strength under the same intermediate principal stress and λ is an empirical coefficient which is a function of σ_2 according to equation 6.

$$\lambda = \frac{\lambda_0}{p\left(\frac{\sigma_2}{\sigma_c}\right)^q + 1} \quad (6)$$

where σ_c is the uniaxial compressive strength of the intact rock, p and q are empirical coefficients and λ_0 is the λ value when the intermediate principal stress equals to zero.

Later He et al. (2016) extended the Kulatilake et al. (2006) criterion to the polyaxial compressive stress condition by equation 7 based on extensive laboratory and numerical polyaxial test results on jointed coal blocks. In equation 7, F_{33} is the fracture tensor component in the minimum principal stress direction.

$$\frac{\sigma_J}{\sigma_I} = e^{-\lambda(F_{22}+F_{33})} \quad (7)$$

They also proposed equation 8 for λ to incorporate the effect of the minimum principal stress, σ_3, as well as the intermediate principal stress. Like equation 6, λ_0 is the λ value for the uniaxial compression condition.

$$\lambda = \frac{\lambda_0}{p_2\left(\frac{\sigma_2}{\sigma_c}\right)^{q_2} + p_3\left(\frac{\sigma_3}{\sigma_c}\right)^{q_3} + 1} \quad (8)$$

where p_2, q_2, p_3 and q_3 are empirical coefficients.

This three-dimensional criterion can predict the strength of jointed rock masses under different confining stresses by estimating the five independent coefficients through regression analyses of the data. Procedures are given in He et al. (2016) in detail to do that. This criterion was developed for non-persistent fracture systems and it captures the effect of scale and anisotropy due to the fracture system on rock mass strength. The proposed criterion by He et al. (2016) can predict the rock mass strength reasonably accurately for non-persistent fracture systems. However, it can be extended to make it suitable for both non-persistent as well as persistent fracture systems. In He et al. (2016) criterion, for a set of constant values of the minimum and intermediate principal stresses σ_2 and σ_3, λ is a constant for a specified rock mass irrespective of the directions of σ_2 and σ_3. When σ_2 and σ_3 directions rotate around the vector normal to the plane of σ_2 and σ_3 (i.e. in σ_1 direction) F_{11} stays as a constant because the first invariant of the fracture tensor ($F_{11} + F_{22} + F_{33}$) is always a constant and thus $F_{22} + F_{33}$ also stays as a constant. Therefore, under the

above-mentioned conditions, Equation 7 provides a constant value and cannot capture the effect of σ_2 on F_{22} and σ_3 on F_{33} separately in predicting rock mass strength. However, this is an important issue to incorporate in predicting rock mass strength especially for persistent fracture systems.

In this research, equations 7 and 8 are extended to capture the effect of σ_2 on F_{22} and σ_3 on F_{33} separately and to develop new rock mass strength criteria based on the results obtained through the jointed rock block modeling and testing under different minimum and intermediate stress combinations and joint geometry systems. The obtained results lead to the following observations:

a) Increase of joint set dip angles, in general, reduce the jointed rock block strength and increase F_{22} and F_{33}. Thus, increase of F_{22} and F_{33} reduce the jointed rock block strength.

b) Increase of the minimum and intermediate principal stresses reduce the effect of joint shearing on the jointed rock block strength. Therefore, increase of the minimum and intermediate principal stresses reduce the effects of F_{22} and F_{33}. However, this reduction for low minimum and intermediate principal stresses is relatively higher compared to high minimum and intermediate principal stresses.

c) The effect of the minimum principal stress on the joints increases with decreasing angle between the dip direction angle of the joint set and the minimum principal stress direction. Thus, increase of F_{33} increases the effect of σ_3 on the joints.

d) The effect of the intermediate principal stress on the joints increases with decreasing angle between the dip direction angle of the joint set and the intermediate principal stress direction. Thus, increase of F_{22} increases the effect of σ_2 on the joints.

Based on the above-mentioned observations the following equation is proposed as a new rock mass strength criterion in a general form.

$$S_r = \frac{\sigma_J}{\sigma_I} = exp - [f_3(\sigma_3/\sigma_c)F_{33} + f_2(\sigma_2/\sigma_c)F_{22}] \quad (9)$$

where f_2 and f_3 are monotonically decreasing functions, S_r is the strength ratio between the jointed rock mass strength, σ_J, under the minimum and intermediate principal stresses of σ_3 and σ_2 and the intact rock strength, σ_I, under the same minimum and intermediate principal stresses, σ_c is the uniaxial compressive strength of the intact rock, F_{22} is the fracture tensor component in σ_2 direction and, F_{33} is the fracture tensor component in σ_3 direction. It should

492 be mentioned that if σ_I for the intended σ_3 and σ_2 combination is not available, based on the Mehranpour and
493 Kulatilake (2016) paper one of the three intact rock failure criteria out of Modified Lade, Modified Wiebols and Cook
494 and Mogi is recommended to represent the intact rock strength value. However, because in this research the intact
495 rock strength for all minimum and intermediate principal stress combinations is available, it is not necessary to use
496 intact rock failure criteria to estimate the intact rock strength.

497 Kulatilake et al. (2006) showed that for the biaxial loading a function such as given by equation 6 works very
498 well for f_2 and f_3. Thus, equation 9 can be rewritten as follows to propose the first new rock mass strength criterion:

499 $$S_r = \frac{\sigma_J}{\sigma_I} = exp - \left[\frac{\lambda_3}{p_3\left(\frac{\sigma_3}{\sigma_c}\right)^{q_3}+1}F_{33} + \frac{\lambda_2}{p_2\left(\frac{\sigma_2}{\sigma_c}\right)^{q_2}+1}F_{22}\right] \quad (10)$$

500 where λ_2, λ_3, p_2, p_3, q_2 and q_3 are empirical coefficients. As an alternative, to reduce the number of coefficients,
501 negative exponential functions are suggested for both f_2 and f_3. Thus, equation 9 can be rewritten as equation 11 with
502 less empirical coefficients to propose the second new rock mass strength criterion.

503 $$S_r = \frac{\sigma_J}{\sigma_I} = exp - \left[a_3\left(e^{-b_3(\sigma_3/\sigma_c)}F_{33}\right) + a_2\left(e^{-b_2(\sigma_2/\sigma_c)}F_{22}\right)\right] \quad (11)$$

504 where a_2, a_3, b_2 and b_3 are empirical coefficients.

505 It should be mentioned that if the joints have the same mechanical properties with isotropic behavior on the
506 joint plane, the effect of σ_2 variation on F_{22} should be the same as the effect of σ_3 variation on F_{33}. Therefore, under
507 this condition $f = f_2 = f_3$ and equations 9-11 can be simplified to equations 12-14, respectively as follows:

508 $$S_r = \frac{\sigma_J}{\sigma_I} = exp - [f(\sigma_3/\sigma_c)F_{33} + f(\sigma_2/\sigma_c)F_{22}] \quad (12)$$

509 $$S_r = \frac{\sigma_J}{\sigma_I} = exp - \lambda\left[\frac{F_{33}}{p\left(\frac{\sigma_3}{\sigma_c}\right)^{q}+1} + \frac{F_{22}}{p\left(\frac{\sigma_2}{\sigma_c}\right)^{q}+1}\right] \quad (13)$$

510 $$S_r = \frac{\sigma_J}{\sigma_I} = exp - a\left[\left(e^{-b(\sigma_3/\sigma_c)}F_{33}\right) + \left(e^{-b(\sigma_2/\sigma_c)}F_{22}\right)\right] \quad (14)$$

511 In equation 12, f is a monotonically decreasing function and in equations 13 and 14, λ, p, q, a and b are empirical
512 coefficients. Moreover, under this condition if $\sigma_2 = \sigma_3$, by rotating the σ_2 and σ_3 directions around the vector normal
513 to the plane of σ_2 and σ_3, the jointed rock mass strength should remain the same. This behavior is also captured by
514 equation 12. If $\sigma_2 = \sigma_3$, equation 12 can be rewritten as follows:

$$S_r = \frac{\sigma_J}{\sigma_I} = exp - [f(\sigma_3/\sigma_c)(F_{33} + F_{22})] \quad (15)$$

where $F_{33} + F_{22}$ is always a constant if σ_2 and σ_3 directions rotate around the vector normal to the plane of σ_2 and σ_3. Therefore, the jointed rock mass strength stays the same under the above-mentioned conditions.

In this research because all the joints are saw cut, they have the same isotropic mechanical behavior on the joint plane. Thus, to fit the new rock mass strength criteria for the numerical modeling results and to find the accuracy of the new rock mass strength criteria equations 13 and 14 can be used. To estimate the values of the coefficients in these equations an indirect method is used. In this method, different values are chosen for empirical coefficients from a grid in a reasonable range. Then the jointed rock mass strength corresponding to different σ_2, σ_3, F_{22} and F_{33} values are calculated through equations 13 and 14. Afterwards, for each equation the best combination of the empirical coefficients is found by maximizing the coefficient of determination, R^2, using the following equations:

$$R^2 = 1 - \frac{S_e}{S_t} \quad (16)$$

where

$$S_e = \frac{1}{n-m-1}\sum_{i=1}^{n}\left(\sigma_{J,i}^{P} - \sigma_{J,i}^{PFC}\right)^2 \quad (17)$$

$$S_t = \frac{1}{n-1}\sum_{i=1}^{n}\left(\sigma_{J,i}^{PFC} - \bar{\sigma}_J^{PFC}\right)^2 \quad (18)$$

where n is the total number of data sets, m is the number of parameters to be estimated, $\sigma_{J,i}^{P}$ is the predicted jointed rock block strength from the new rock mass strength criterion for data set i, $\sigma_{J,i}^{PFC}$ is the strength of jointed rock block from the PFC^{3D} modeling for data set i, and $\bar{\sigma}_J^{PFC}$ is the average strength value of all the PFC^{3D} data.

4.1. Fitting of the first new rock mass strength criterion using equation 13

In Fig. 16, the obtained R^2 values are shown for different values of p and q for selected 3 different λ values. The maximum R^2 is found to be 0.94, indicating a very strong fit. It results in the best values of 0.675, 3.16 and 0.6, for λ, p and q, respectively. Fig. 17 shows the predicted strength values versus the strength values from the PFC^{3D} modeling for all 284 data points. It indicates that the suggested strength criterion (eqn. 13) is highly suitable to represent the PFC^{3D} data.

4.2. Fitting of the second new rock mass strength criterion using equation 14

In Fig. 18, the obtained R^2 values are shown for different values of *a* and *b* for the 284 data points from 12 different joint systems under the different minimum and intermediate principal stress combinations. The maximum R^2 is found to be 0.92. It results in the best values of 0.404 and 0.972, for *a* and *b*, respectively. The small difference obtained between the R^2 values using the two different functions shows that equation 14 with less empirical coefficients is also a reasonably good rock mass strength criterion. Fig. 19 shows the predicted strength values based on equation 14 versus the strength values from the PFC^{3D} modeling for all 284 data points. It indicates that the suggested strength criterion (eqn. 14) is highly suitable to represent the PFC^{3D} data. Fig. 20 shows the comparison between the predicted rock mass strengths from the new rock mass strength criteria using equations 13 and 14 with the numerical results for two different joint systems with one and two joint sets, respectively. Fig. 20 shows that the predictions from the two strength criteria are close.

5. Discussion

The equations given in Section 4 to estimate the jointed block strength for synthetic rock are normalized with respect to the synthetic intact rock strength. Therefore, the equations are applicable for any rock mass. The equations allow to estimate the normalized jointed block strength in any direction in three dimensions. By estimating the strength in different directions, the strength anisotropy and the minimum normalized jointed block strength can be estimated in three dimensions. The intact block strength can be estimated using one of the available intact rock strength criteria. To estimate the parameters of the intact rock strength criterion, it will be necessary to perform a few laboratory tests as usual. To apply the equations given for normalized jointed block strength for any rock mass, first, the fracture geometry data (number of fracture sets and orientation, size and intensity of each set) should be collected for the intended rock mass. These data can be used to calculate the fracture tensor using equations 3 and 4 as shown in Table 6. That will allow calculation of the two fracture tensor components perpendicular to the direction jointed block strength is desired. These two fracture tensor components go into the normalized jointed block strength equation. The confining stresses should be applied based on the in-situ stress system. For the time being the estimated coefficient values of the equations can be used to estimate the jointed block strength. It is important to note that these coefficient values depend on the ratios of joint mechanical property values to intact rock property values. This dependence should be investigated in future research.

6. Summary and Conclusions

In this research an attempt was made to develop a new three-dimensional rock mass strength criterion to overcome the shortcomings that exist in most of the existing rock mass strength criteria. Most of the existing strength criteria cannot simultaneously consider the effect of the intermediate principal stress on the rock mass strength as well as the scale dependency and anisotropy behavior of the rock mass strength. Although He et al. (2016) proposed a three-dimensional criterion which captures the effect of the intermediate principal stress, scale dependency and anisotropy due to the fracture system on rock mass strength their criterion did not incorporate the effect of the stress anisotropy because it was developed for non-persistent fracture systems. Besides, He et al. (2016) criterion requires calibration of five empirical coefficients. However, the stress anisotropy is important especially in the case of fully persistent fracture systems (Mehranpour and Kulatilake 2017). Therefore, in this paper the He et al. (2016) criterion was extended to incorporate the effect of stress anisotropy too and to develop two new rock mass strength criteria.

To develop a comprehensive rock mass strength criterion, it is crucial to have a proper database which includes the effect of different factors such as the joint geometry configuration including the orientation and the minimum and intermediate principal stresses. Due to the high cost and time of the experimental tests, it is very difficult if not impractical to have a comprehensive database only through experimental tests. Therefore, numerical modeling was incorporated to create this database. The other benefit of the numerical modeling is the possibility to investigate the effect of each factor separately while keeping the values of the other factors the same. In this research, PFC^{3D} was selected for the numerical modeling because it can conveniently model the block breakage through the fracture initiation and propagation using the Bonded Particle Models and joint failure through the joint sliding using the SJCM. In this paper, because of the shortcoming of the SJCM to capture the non-linear behavior of the joint closure due to varying joint normal stress, the MSJCM was used. Moreover, to solve the interlocking problem which occurs due to the shortcoming of the PFC software in the updating procedure of the contact conditions of the particles that lie around the intended joint plane during high shear displacements, the JSC approach was used.

Before simulating the jointed rock blocks under the polyaxial, triaxial and biaxial compression tests, these tests were simulated on the synthetic intact rock samples to find the intact rock strength for selected minimum and intermediate principal stress combinations. Altogether 33 intact rock strength values for different combinations of minimum and intermediate principal stresses were obtained from the numerical modeling for the synthetic intact rock. Then, 12 different joint systems with one and two joint sets were chosen to model the jointed rock blocks under the polyaxial, triaxial and biaxial compression tests with the minimum and intermediate principal stress combinations

similar to those conducted for the intact rock modeling. Used joint sets have different dip angles varying from 15° to 45° at an interval of 15° with dip directions of 30° and 75°. Each joint set also has 3 persistent joints with the joint spacing of 42 mm in a cubic sample of size 160 mm. In total 284 jointed block strengths were obtained from the numerical modeling of the jointed rock blocks. It should be mentioned that because the numerical and experimental test results of polyaxial and triaxial compression tests on the synthetic intact rock and jointed rock blocks showed a reasonable agreement, it was not necessary to update the micro mechanical properties of the calibrated PFC^{3D} model.

Based on the observations from the jointed rock modeling results using PFC^{3D} and the fracture tensor concept, an existing rock mass strength criterion was extended to include the stress anisotropy and to develop a new three-dimensional rock mass strength criterion in general form (equation 9). For the new general rock mass strength criterion, two functions were proposed: (a) given by equation 10 and (b) given by equation 11 to obtain two specific new rock mass strength criteria. The new rock mass strength criterion given by equation 10 has 6 empirical coefficients; if the joint sets have the same isotropic mechanical behavior on the joint plane, the number of coefficients reduces to 3 empirical coefficients in this criterion (equation 13). The new rock mass strength criterion given by equation 11 has only 4 empirical coefficients; if the joint sets have the same isotropic mechanical behavior on the joint plane the number of coefficients reduces to 2 empirical coefficients in this criterion (equation 14).

Using the database created in this paper, which has 284 data points, the empirical coefficients of λ, p and q were estimated as 0.675, 3.16 and 0.6, respectively, through a grid analysis with a high R^2 value of 0.94 for the new criterion given by equation 13. The empirical coefficients of a and b were estimated as 0.404 and 0.972, respectively, through a grid analysis with a high R^2 value of 0.92 for the new criterion given by equation 14. Even though the first criterion was fitted with a slightly higher R^2 value than the second criterion, it was less time consuming and significantly easier to estimate the empirical coefficients for the second criterion. Both new criteria clearly showed the effect of the intermediate principal stress as well as the minimum principal stress and joint orientation on the rock mass strength. Because the developed jointed block strength criteria are expressed in normalized form by dividing by the intact block strength, the normalized jointed block strength criteria are applicable for any rock mass. Guidelines are given to show how the developed strength criteria can be applied to field rock masses.

Acknowledgements

620 The research was funded by the National Institute for Occupational Safety, and Health (NIOSH) of the Centers for
621 Disease Control, and Prevention (Contract No. 200-2011-39886).

622 **References**

623 Amadei B (1996) Importance of anisotropy when estimating and measuring in situ stresses in rock. Int J Rock Mech
624 Min Sci 33(3):293-325. http://dx.doi.org/10.1016/0148-9062(95)00062-3
625
626 Bahaaddini M, Hagan PC, Mitra R, Hebblewhite BK (2015) Parametric study of smooth joint parameters on the shear
627 behaviour of rock joints. Rock Mech Rock Eng 48(3):923-940. http://dx.doi.org/10.1007/s00603-014-0641-6
628
629 Bahaaddini M, Sharrock G, Hebblewhite BK (2013) Numerical direct shear tests to model the shear behaviour of rock
630 joints. Comput Geotech 51:101-115. http://dx.doi.org/10.1016/j.compgeo.2013.02.003
631
632 Bandis SC, Lumsden AC, Barton NR (1983) Fundamentals of rock joint deformation. Int J Rock Mech Min Sci
633 Geomech 20(6):249–68. http://dx.doi.org/10.1016/0148-9062(83)90595-8
634
635 Barton N, Lien R, Lunde J (1974) Engineering classification of rock masses for the design of tunnel support Rock
636 Mech Rock Eng 6(4):189-236. http://dx.doi.org/10.1007/BF01239496
637
638 Bekaert A, Maghous S (1996) Three-dimensional yield strength properties of jointed rock mass as a homogenized
639 medium. Mech Cohes-Frict Mat 1(1):1-24. http://dx.doi.org/10.1002/(SICI)1099-1484(199601)1:1<1::AID-
640 CFM1>3.0.CO;2-O
641
642 Bieniawski ZT (1973) Engineering classification of jointed rock masses. Trans S Afr Inst Civ Eng 15:335-344
643
644 Chiu CC, Wang TT, Weng MC, Huang TH (2013) Modeling the anisotropic behavior of jointed rock mass using a
645 modified smooth-joint model. Int J Rock Mech Min Sci 62:14-22. http://dx.doi.org/10.1016/j.ijrmms.2013.03.011
646

Cho NA, Martin CD, Sego DC (2007) A clumped particle model for rock. Int J Rock Mech Min Sci 44(7):997-1010. http://dx.doi.org/10.1016/j.ijrmms.2007.02.002

Colak K, Unlu T (2004) Effect of transverse anisotropy on the Hoek–Brown strength parameter 'm_i'for intact rocks. Int J Rock Mech Min 41(6):1045-52. https://doi.org/10.1016/j.ijrmms.2004.04.004

Cundall PA, Hart RD (1992) Numerical modelling of discontinua. Eng computations 9(2):101-113. http://dx.doi.org/10.1108/eb023851

Cundall PA, Strack OD (1979) A discrete numerical model for granular assemblies. Geotechnique 29(1):47-65

Duan K, Kwok CY (2016) Evolution of stress-induced borehole breakout in inherently anisotropic rock: Insights from discrete element modeling. Journal Geophys Res-Sol Ea 121(4):2361-2381. http://dx.doi.org/10.1002/2015JB012676

Fakhimi A (2004) Application of slightly overlapped circular particles assembly in numerical simulation of rocks with high friction angles. Eng Geol 74(1):129-138. http://dx.doi.org/10.1016/j.enggeo.2004.03.006

Fan X, Kulatilake PHSW, Chen X (2015) Mechanical behavior of rock-like jointed blocks with multi-non-persistent joints under uniaxial loading: a particle mechanics approach. Eng Geol 190:17-32. http://dx.doi.org/10.1016/j.enggeo.2015.02.008

Gigli G, Casagli N (2011) Semi-automatic extraction of rock mass structural data from high resolution LIDAR point clouds. Int J Rock Mech Min Sci 48(2):187-198. http://dx.doi.org/10.1016/j.ijrmms.2010.11.009

Goel RK, Singh B (2011) Engineering rock mass classification: tunnelling, foundations and landslides: Elsevier Inc.

Goodman RE (1976) Methods of geological engineering in discontinuous rocks.

675 He PF, Kulatilake PHSW, Liu DQ, He MC (2016) Development of a New Three-Dimensional Coal Mass Strength
676 Criterion. International Journal of Geomechanics 17(3):04016067. http://dx.doi.org/10.1061/(ASCE)GM.1943-
677 5622.0000741
678
679 Hoek E (1994) Strength of rock and rock masses. ISRM News Journal 2(2):4-16
680
681 Ismael MA, Imam HF, El-Shayeb Y (2014) A simplified approach to directly consider intact rock anisotropy in Hoek–
682 Brown failure criterion. J Rock Mech Geot Eng 6(5):486-92. https://doi.org/10.1016/j.jrmge.2014.06.003
683
684 Itasca Consulting Group Inc. (2016) PFC manual, version 5.0, Minneapolis.
685
686 Koyama T, Jing L (2007) Effects of model scale and particle size on micro-mechanical properties and failure processes
687 of rocks- A particle mechanics approach. Eng Anal Bound Elem 31(5):458-472.
688 http://dx.doi.org/10.1016/j.enganabound.2006.11.009
689
690 Kulatilake PHSW (1985) Estimating elastic constants and strength of discontinuous rock. J Geotech Eng, ASCE
691 111(7):847-864. http://dx.doi.org/10.1061/(ASCE)0733-9410(1985)111:7(847)
692
693 Kulatilake PHSW (2016) Physical, empirical and numerical modeling of jointed rock mass strength. Invited Book
694 Chapter, In: Feng XT, Hudson J, editors. Rock Mechanics and Engineering, CRC Press, Balkema, Taylor and Francis
695 Group.
696
697 Kulatilake PHSW, Malama B, Wang J (2001) Physical and particle flow modeling of jointed rock block behavior
698 under uniaxial loading. Int J Rock Mech Min 38(5):641-57. http://dx.doi.org/10.1016/S1365-1609(01)00025-9
699
700 Kulatilake PHSW, Park J, Malama B (2006) A new rock mass failure criterion for biaxial loading conditions. Geotech
701 Geol Eng 24(4):871-88. http://dx.doi.org/10.1007/s10706-005-7465-9
702

703 Kulatilake PHSW, Shreedharan S, Sherizadeh T, Shu B, Xing Y, He P (2016) Laboratory estimation of rock joint
704 stiffness and frictional parameters. Geotech Geol Eng 34(6): 1723–1735. http://dx.doi.org/10.1007/s10706-016-9984-
705 y
706
707 Kulatilake PHSW, Shu B (2015) Prediction of rock mass deformations in three dimensions for a part of an open pit
708 mine and comparison with field deformation monitoring data. Geotech Geol Eng 33:1551-1568.
709 http://dx.doi.org/10.1007/s10706-015-9921-5
710
711 Kulatilake PHSW, Wang S, Stephansson O (1993) Effect of finite size joints on deformability of jointed rock at the
712 three dimensional level. Int J Rock Mech Min Sci 30(5):479-501. http://dx.doi.org/10.1016/0148-9062(93)92216-D
713
714 Lee H, Jeon S (2011) An experimental and numerical study of fracture coalescence in pre-cracked specimens under
715 uniaxial compression. Int J Solids Struct 48:979-999. http://dx.doi.org/10.1016/j.ijsolstr.2010.12.001
716
717 Malama B, Kulatilake PHSW (2003) Models for normal fracture deformation under compressive loading. Int J Rock
718 Mech Min Sci 40(6):893-901. http://dx.doi.org/10.1016/S1365-1609(03)00071-6
719
720 Marinos V, Marinos P, Hoek E (2005) The geological strength index: applications and limitations. B Eng Geol Environ
721 64(1):55-65. http://dx.doi.org/10.1007/s10064-004-0270-5
722
723 Mas Ivars D, Pierce ME, Darcel C, Reyes-Montes J, Potyondy DO, Young RP, Cundall PA (2011) The synthetic rock
724 mass approach for jointed rock mass modelling. Int J Rock Mech Min Sci 48(2):219-244.
725 http://dx.doi.org/10.1016/j.ijrmms.2010.11.014
726
727 Mehranpour MH, Kulatilake PHSW (2016) Comparison of six major intact rock failure criteria using a particle flow
728 approach under true-triaxial stress condition. Geomech Geophy Geo-energ Geo-resour 2(4):203-229.
729 http://dx.doi.org/10.1007/s40948-016-0030-6
730

731 Mehranpour MH, Kulatilake PHSW (2017) Improvements for the smooth joint contact model of the particle flow code
732 and its applications. Comput Geotech 87:163-77. https://doi.org/10.1016/j.compgeo.2017.02.012
733
734 Melkoumian N, Priest SD, Hunt SP (2009) Further development of the three-dimensional Hoek–Brown yield criterion.
735 Rock Mech Rock Eng 42(6):835-47. https://doi.org/10.1007/s00603-008-0022-0
736
737 Oda M (1982) Fabric tensor for discontinuous geological materials. Soils and Foundations, 22(4): 96–108.
738 http://doi.org/10.3208/sandf1972.22.4_96
739
740 Oda M (1984) Similarity rule of crack geometry in statistically homogeneous rock masses. Mechanics of Materials.
741 3(2):119-29. http://dx.doi.org/10.1016/0167-6636(84)90003-6
742
743 Pan XD, Hudson JA (1988) A simplified three dimensional Hoek-Brown yield criterion. In ISRM International
744 Symposium. International Society for Rock Mechanics
745
746 Park JW, Song JJ (2009) Numerical simulation of a direct shear test on a rock joint using a bonded-particle model. Int
747 J Rock Mech Min Sci 46(8):1315-1328. http://dx.doi.org/10.1016/j.ijrmms.2009.03.007
748
749 Pierce M, Cundall P, Potyondy D, Mas Ivars D (2007) A synthetic rock mass model for jointed rock. In: Eberhardt E,
750 Stead D, Morrison T, editors. Rock Mechanics: Meeting Society's Challenges and Demands. Proceeding of the 1st
751 Canada-US Rock Mechanics Symposium; May 27-31 Vancouver, Canada. London: Taylor & Francis Group. 1:341-
752 349
753
754 Potyondy DO (2015) The bonded-particle model as a tool for rock mechanics research and application: current trends
755 and future directions. Geosyst Eng 18(1):1-28.http://dx.doi.org/10.1080/12269328.2014.998346
756
757 Potyondy DO, Cundall PA (2004) A bonded-particle model for rock. Int J Rock Mech Min Sci 41(8):1329-1364.
758 http://dx.doi.org/10.1016/j.ijrmms.2004.09.011

759

760 Pouya A, Ghoreychi M (2001) Determination of rock mass strength properties by homogenization. Int J Numer and
761 Anal Met 25(13):1285-1303. http://dx.doi.org/10.1002/nag.176

762

763 Priest SD (2005) Determination of shear strength and three-dimensional yield strength for the Hoek-Brown criterion.
764 Rock Mech Rock Eng 38(4):299-327. https://doi.org/10.1007/s00603-005-0056-5

765

766 Ramamurthy T (2001) Shear strength response of some geological materials in triaxial compression. Int J Rock Mech
767 Min 38(5):683-97. https://doi.org/10.1016/S1365-1609(01)00035-1

768

769 Saroglou H, Tsiambaos G (2008) A modified Hoek–Brown failure criterion for anisotropic intact rock Int J Rock
770 Mech Min 45(2):223-34. https://doi.org/10.1016/j.ijrmms.2007.05.004

771

772 Schöpfer MP, Childs C, Manzocchi T (2013) Three-dimensional failure envelopes and the brittle-ductile transition. J
773 Geophys Res-Sol Ea 118(4):1378-1392. http://dx.doi.org/10.1002/jgrb.50081

774

775 Shehata WM (1972) fundamental considerations on the hydraulic characteristics of joints in rock. In: Proceedings of
776 the Symposium on Percolation Through Fissured Rock; Sep 18-19; Stuttgart, Germany. paper (No. T1-F)

777

778 Sheorey PR, Biswas A, Choubey VD (1989) An empirical failure criterion for rocks and jointed rock masses. Eng
779 Geol 26(2):141-59. https://doi.org/10.1016/0013-7952(89)90003-3

780

781

782 Shreedharan S, Kulatilake PHSW (2016) Discontinuum–equivalent continuum analysis of the stability of tunnels in a
783 deep coal mine using the distinct element method. Rock Mech Rock Eng 49(5):1903-1922.
784 http://dx.doi.org/10.1007/s00603-015-0885-9

785

786 Swan G (1983) Determination of stiffness and other joint properties from roughness measurements. Rock Mech Rock
787 Eng 16(1):19-38. http://dx.doi.org/10.1007/BF01030216
788
789
790 Wu Q, Kulatilake PHSW (2012) REV and its properties on fracture system and mechanical properties, and an
791 orthotropic constitutive model for a jointed rock mass in a dam site in China. Comput Geotech 43:124-142.
792 http://dx.doi.org/10.1016/j.compgeo.2012.02.010
793
794
795 Yang X, Kulatilake PHSW, Jing H, Yang S (2015) Numerical simulation of a jointed rock block mechanical behavior
796 adjacent to an underground excavation and comparison with physical model test results. Tunn Undergr Sp Tech
797 50:129-142. http://dx.doi.org/10.1016/j.tust.2015.07.006
798
799 Yu, Q (2001) Computational simulations of shear behavior of joints in brittle geomaterials. Doctoral dissertation,
800 McGill University, Montreal.
801
802 Yudhbir Y, Lemanza W, Prinzl F (1983) An empirical failure criterion for rock masses. In 5th ISRM Congress.
803 International Society for Rock Mechanics
804
805 Zhang L (2008) A generalized three-dimensional Hoek–Brown strength criterion. Rock Mech Rock Eng 41(6):893-
806 915. https://doi.org/10.1007/s00603-008-0169-8
807
808 Zhang L, Zhu H (2007) Three-dimensional Hoek-Brown strength criterion for rocks. J Geotech Geoenviron
809 133(9):1128-35. https://doi.org/10.1061/(ASCE)1090-0241(2007)133:9(1128)
810
811 Zhang Q, Zhu H, Zhang L (2013) Modification of a generalized three-dimensional Hoek–Brown strength criterion.
812 Int J Rock Mech Min 59:80-96. https://doi.org/10.1016/j.ijrmms.2012.12.009
813

814 Zhang Y, Stead D, Elmo D (2015) Characterization of strength and damage of hard rock pillars using a synthetic rock
815 mass method. Comput Geotech 65:56-72. http://dx.doi.org/10.1016/j.compgeo.2014.12.002
816
817 Zheng J, Kulatilake PHSW, Shu B, Sherizadeh T, Deng J (2014) Probabilistic block theory analysis for a rock slope
818 at an open pit mine in USA, Comput Geotech 61:254-265. http://dx.doi.org/10.1016/j.compgeo.2014.06.002
819
820
821
822
823
824
825
826
827
828
829
830
831
832
833
834
835
836
837
838
839
840
841

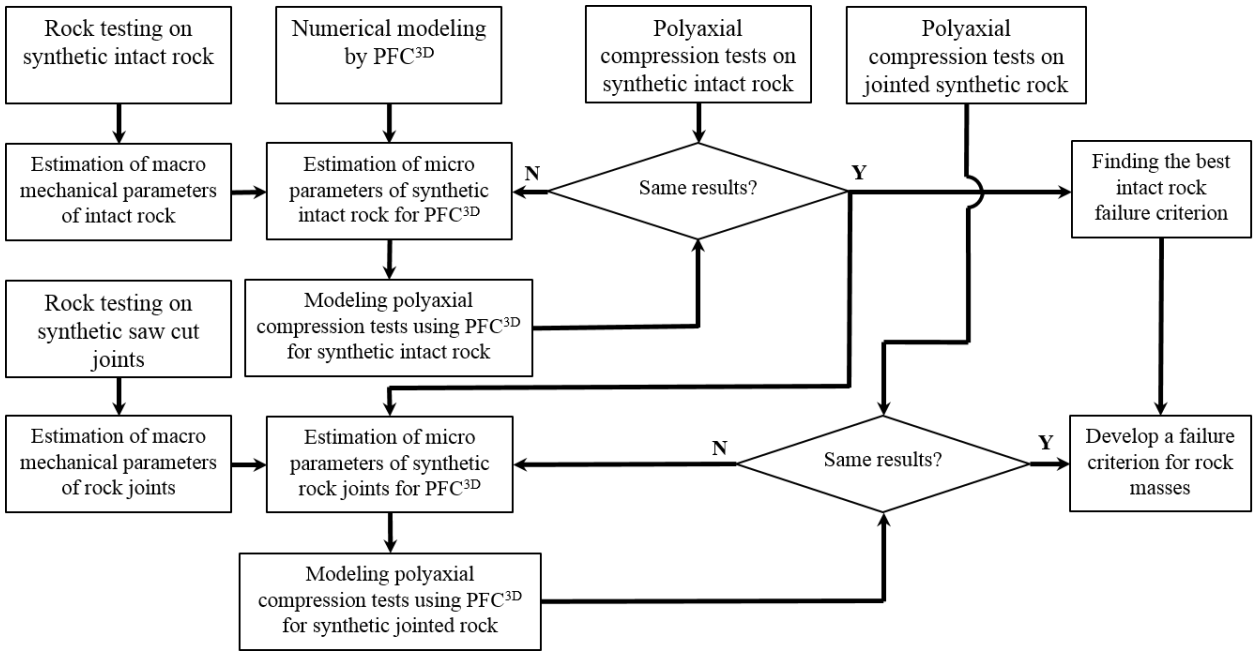

842

843 **Fig. 1** Used flowchart to develop a new rock mass failure criterion

844

845

846 **Fig. 2** The polyaxial testing machine available at CUMTB

847

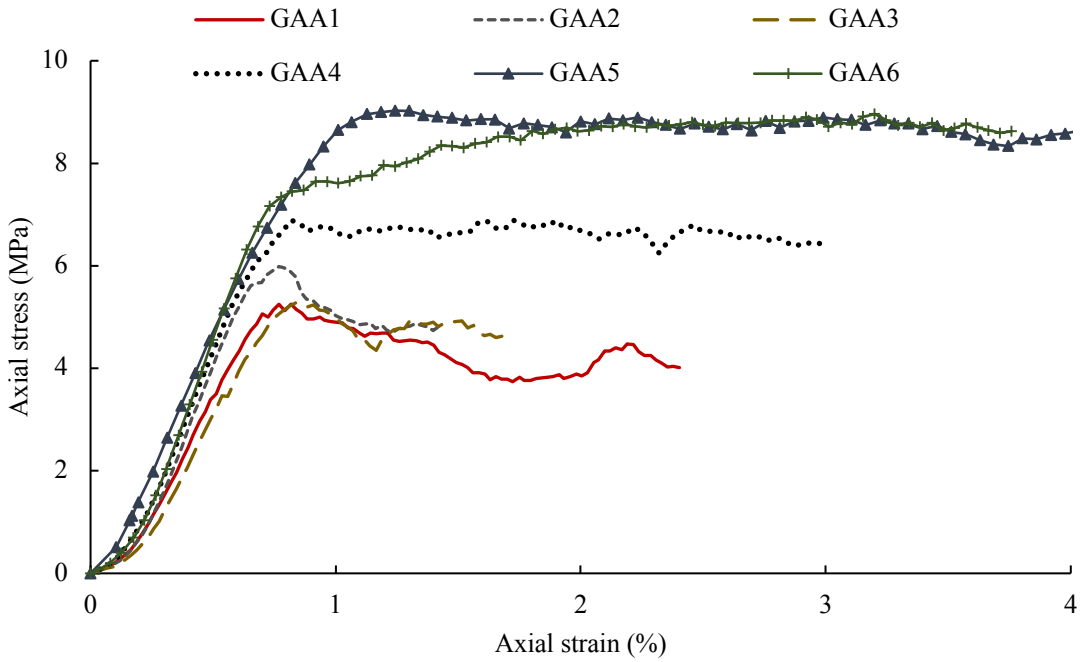

848

849 **Fig. 3** Uniaxial and triaxial test results; GAA1, GAA2 and GAA3 ($\sigma_2 = \sigma_3 = 0$); GAA4 ($\sigma_2 = \sigma_3 = 0.53$
850 MPa); GAA5 ($\sigma_2 = \sigma_3 = 1.11$ MPa); GAA6 ($\sigma_2 = \sigma_3 = 1.64$ MPa)

851

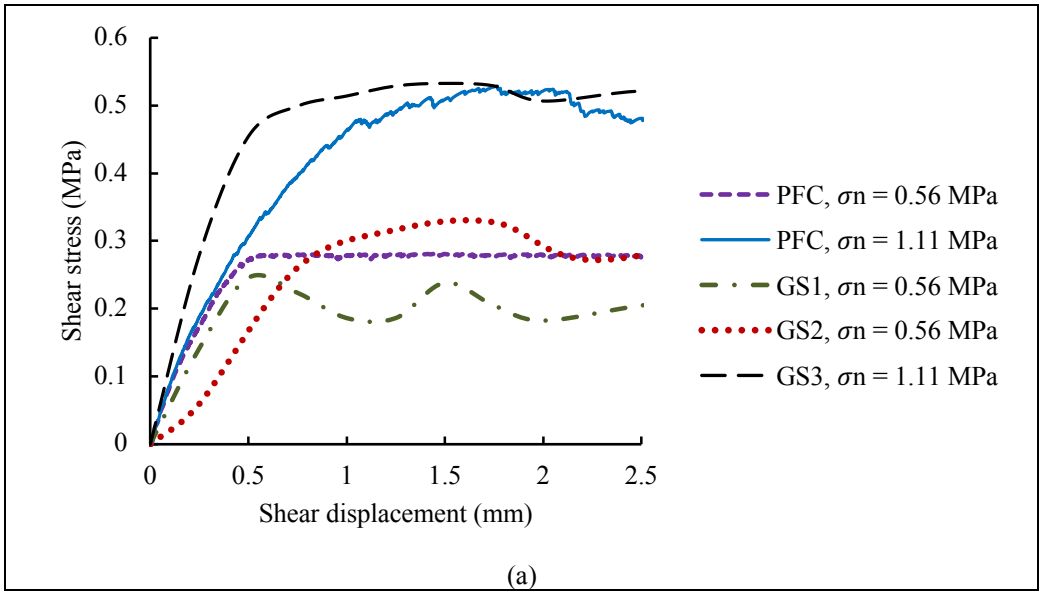

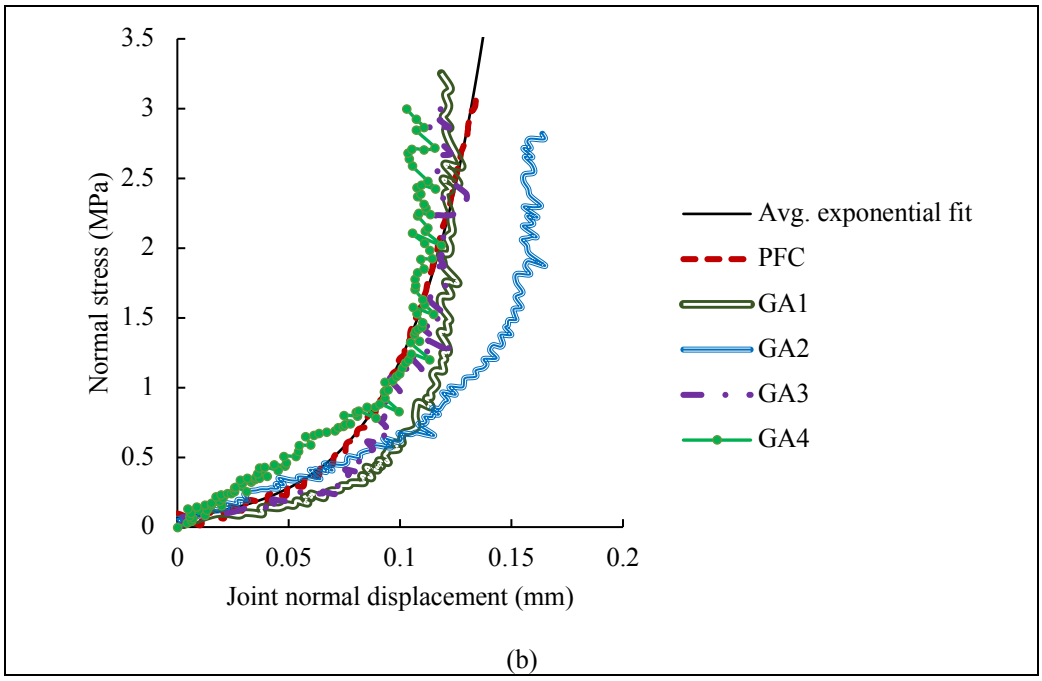

852

853 **Fig. 4** (a) Shear stress-shear displacement diagrams for 3 direct shear tests, and PFC modeling results; (b)
854 normal stress-joint normal deformation diagrams based on 4 experimental jointed uniaxial compression test
855 results, the average of the exponential fit for normal stress-joint normal deformation relation, and PFC
856 modeling result based on the Modified Smooth Joint Contact Model

857

858

859

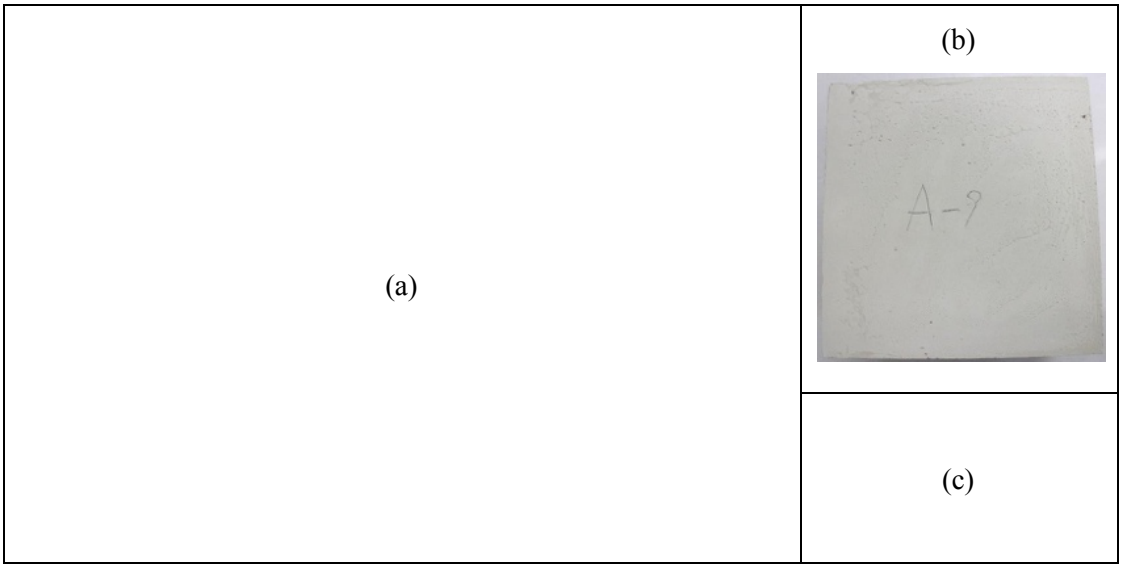

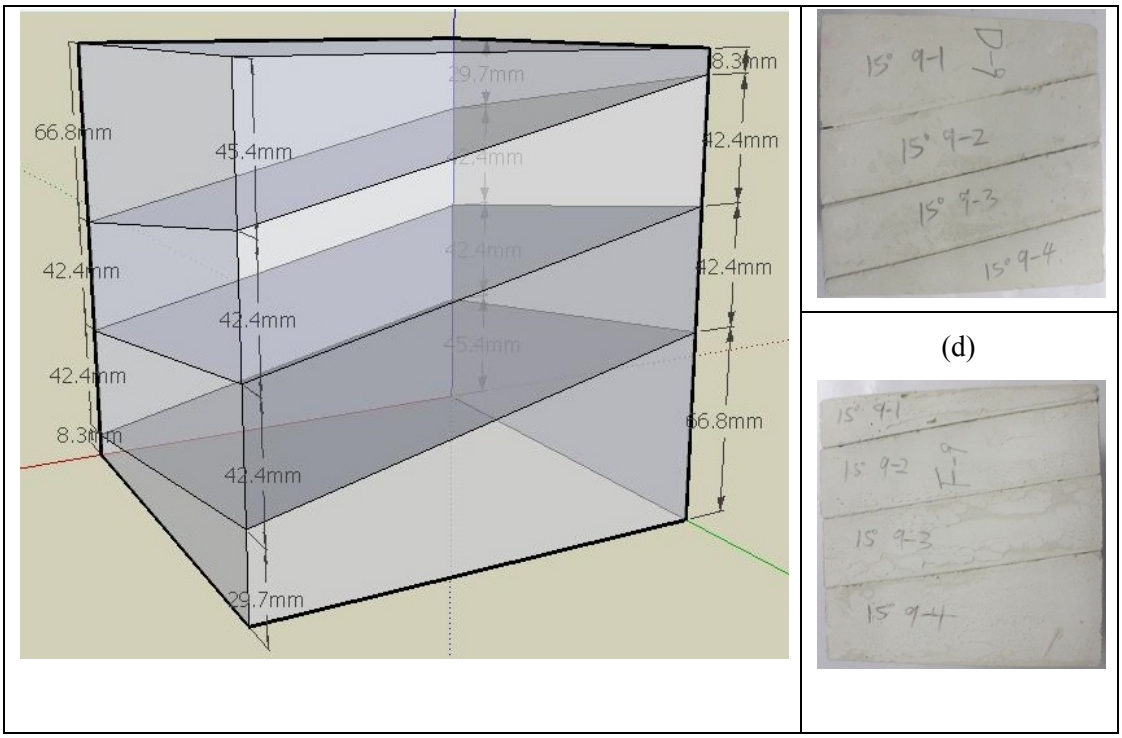

Fig. 5 Jointed rock block sample which has 3 joints with the dip direction of 30° and the dip angle of 15°: (a) Schematic picture and the (b) top, (c) left front and (d) right front views of a prepared sample for the experimental test (the maximum principal stress applied on the top face, the intermediate principal stress applied on the left front face and the minimum principal stress applied on the right front face)

(a)	(b)

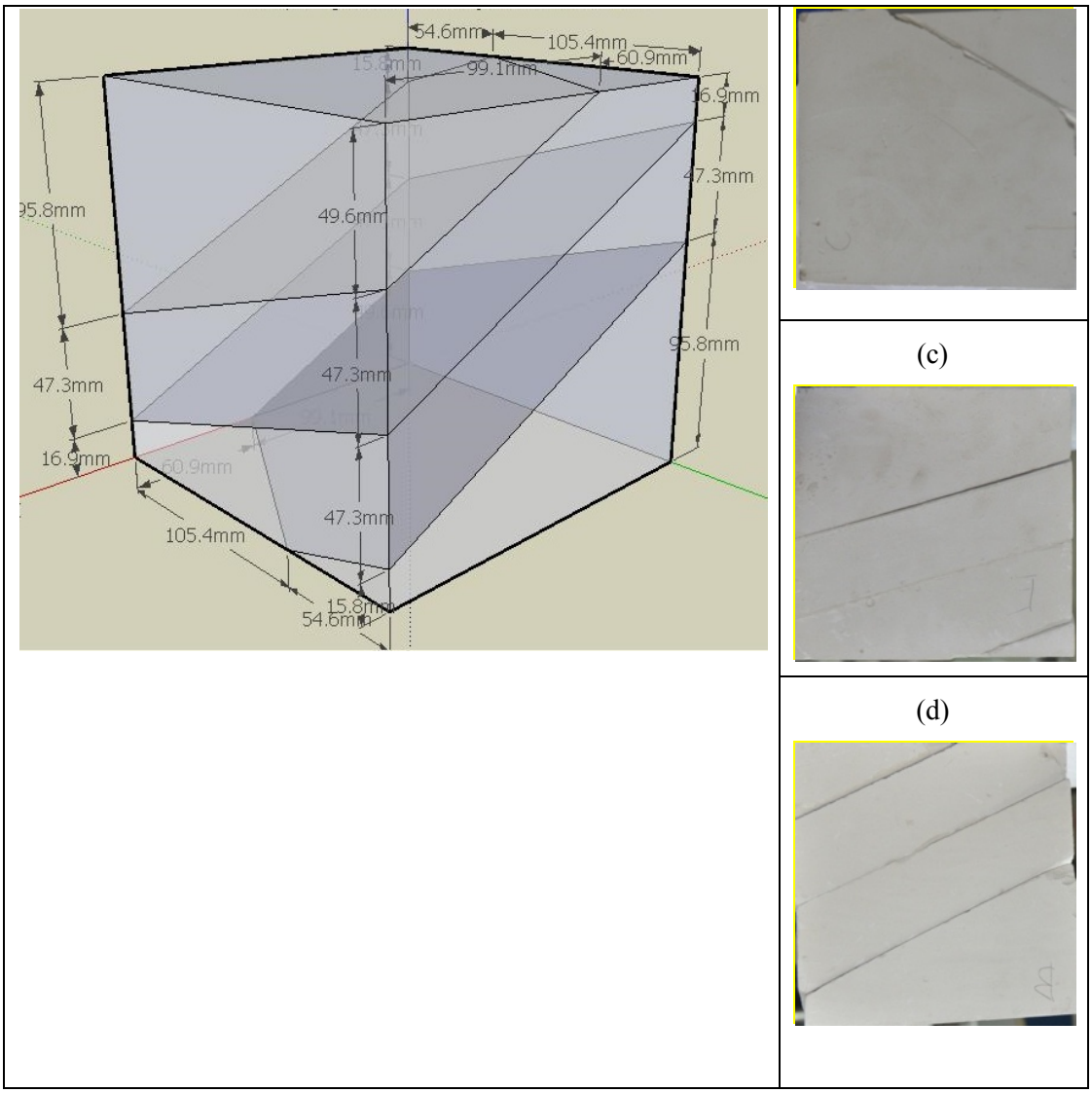

873

874 **Fig. 6** Jointed rock block sample which has 3 joints with the dip direction of 30° and the dip angle of 30°:
875 (a) Schematic picture and the (b) top, (c) left front and (d) right front views of a prepared sample for the
876 experimental test (the maximum principal stress applied on the top face, the intermediate principal stress
877 applied on the left front face and the minimum principal stress applied on the right front face)

878

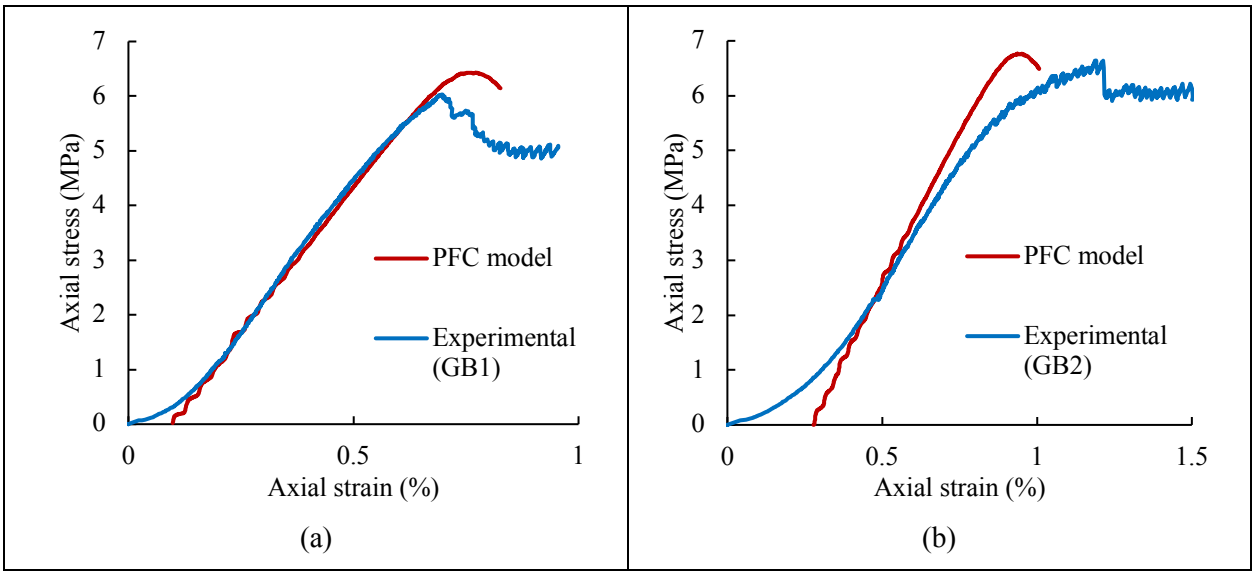

879

880 **Fig. 7** Experimental and PFC^{3D} modeling results of the polyaxial compression test for the intact rock
881 subjected to (a) $\sigma_3 = 0$ and $\sigma_2 = 1.128$ MPa, (b) $\sigma_3 = 0$ MPa and $\sigma_2 = 2.256$ MPa

882

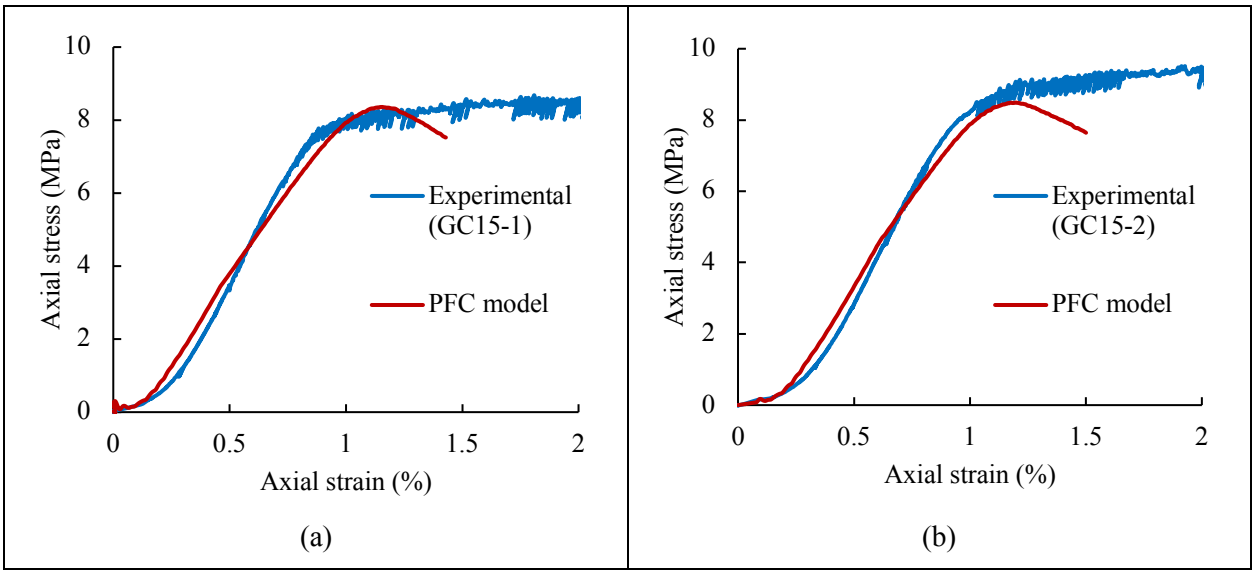

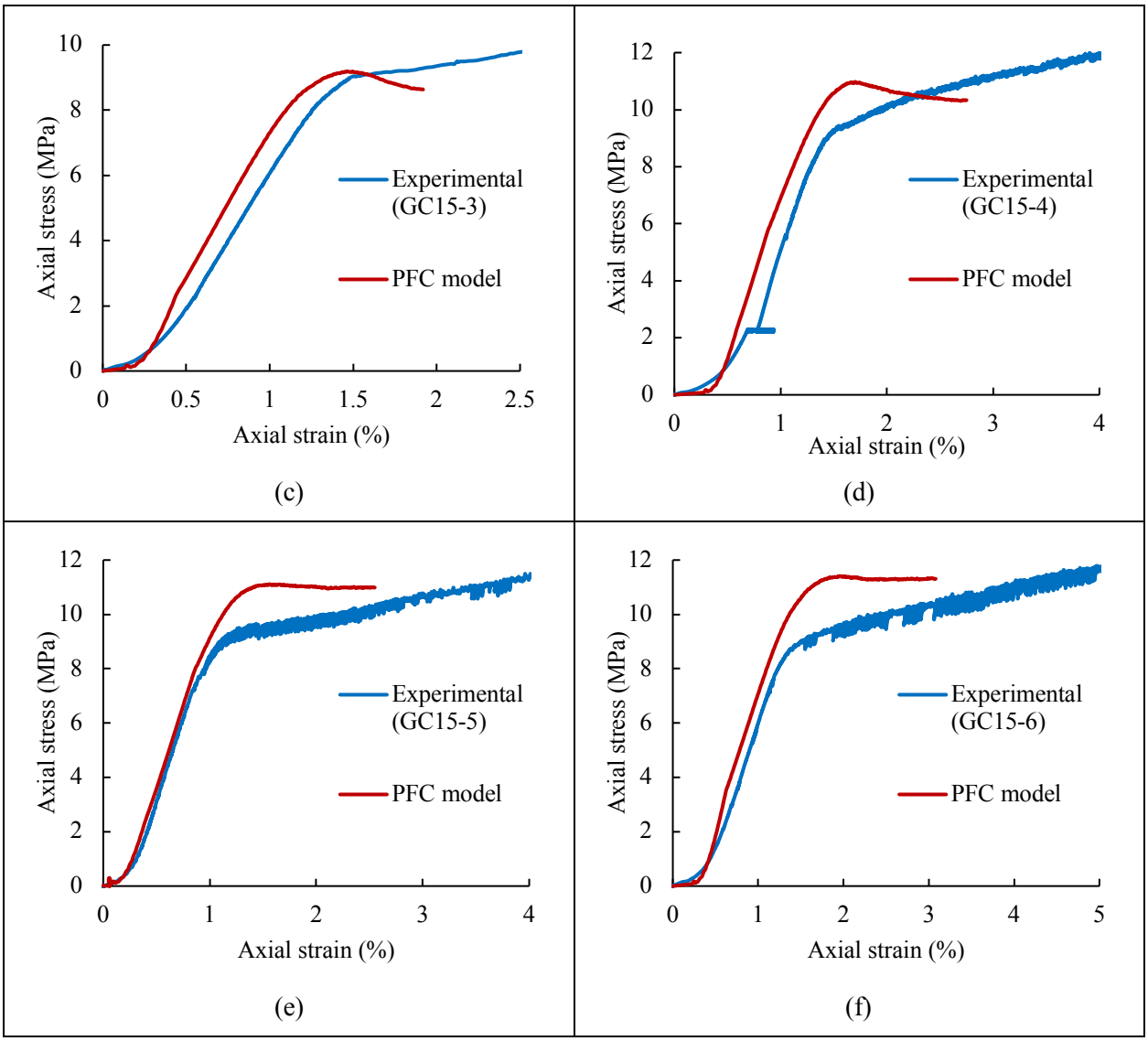

Fig. 8 Experimental and PFC^{3D} modeling results of the polyaxial and triaxial compression tests for the jointed rock block samples having one joint set with the joint dip direction of 30° and dip angle of 15° subjected to (a) $\sigma_3 = 1.128$ MPa and $\sigma_2 = 3.384$ MPa, (b) $\sigma_3 = 1.128$ MPa and $\sigma_2 = 4.512$ MPa, (c) $\sigma_3 = \sigma_2 = 2.256$ MPa, (d) $\sigma_3 = 2.256$ MPa and $\sigma_2 = 4.512$ MPa, (e) $\sigma_3 = 2.256$ MPa and $\sigma_2 = 7.896$ MPa and (f) $\sigma_3 = \sigma_2 = 3.384$ MPa

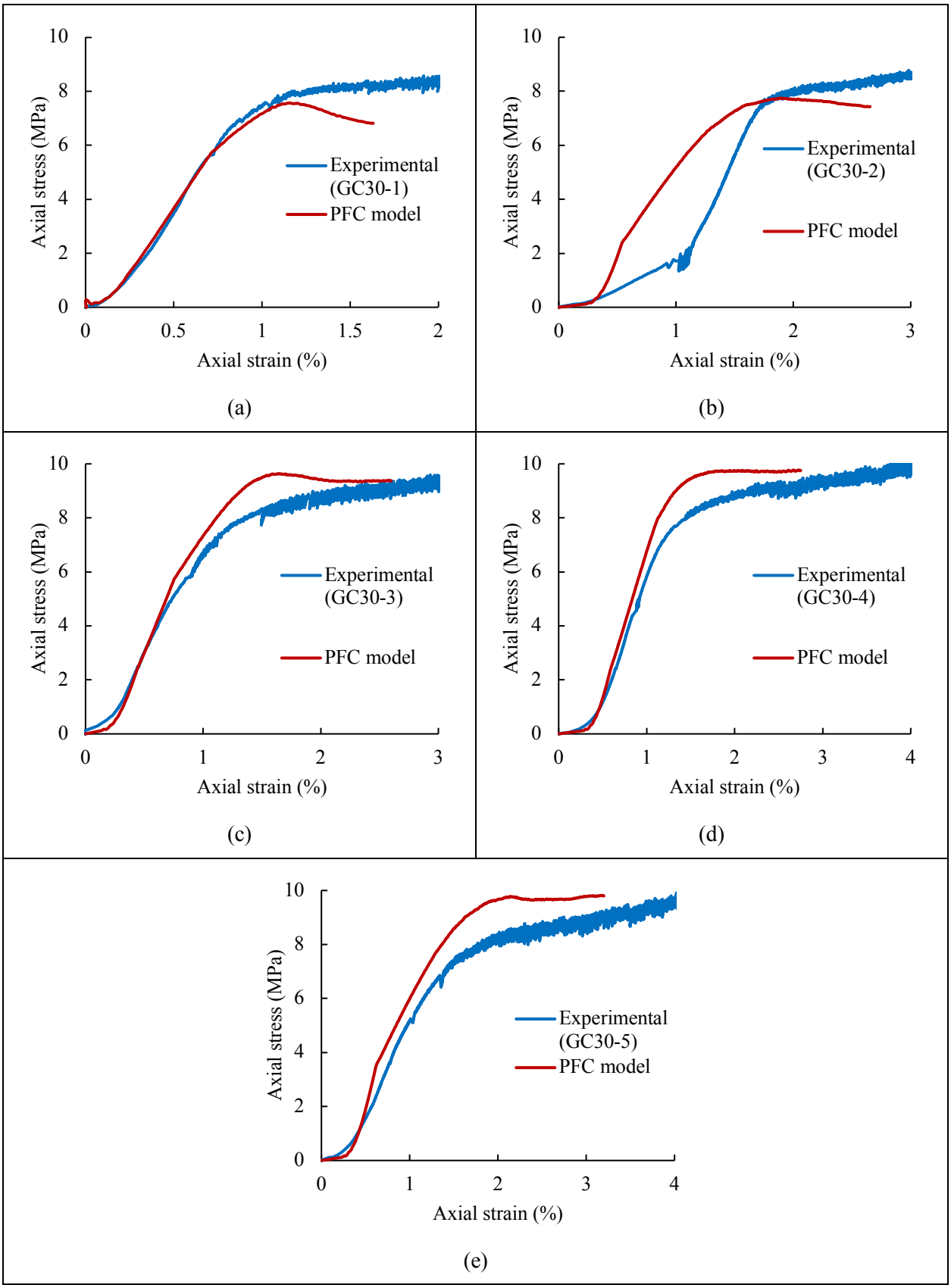
Axial stress (MPa)
Axial strain (%)
Experimental (GC30-1)
PFC model
(a)
Experimental (GC30-2)
PFC model
(b)
Experimental (GC30-3)
PFC model
(c)
Experimental (GC30-4)
PFC model
(d)
Experimental (GC30-5)
PFC model
(e)

Fig. 9 Experimental and PFC^{3D} modeling results of the polyaxial and triaxial compression tests for the jointed rock samples having one joint set with the joint dip direction of 30° and dip angle of 30° subjected to (a) $\sigma_3 = 1.128$ MPa and $\sigma_2 = 5.640$ MPa, (b) $\sigma_3 = \sigma_2 = 2.256$ MPa, (c) $\sigma_3 = 2.256$ MPa and $\sigma_2 = 5.640$ MPa, (d) $\sigma_3 = 2.256$ MPa and $\sigma_2 = 7.896$ MPa and (e) $\sigma_3 = \sigma_2 = 3.384$ MPa

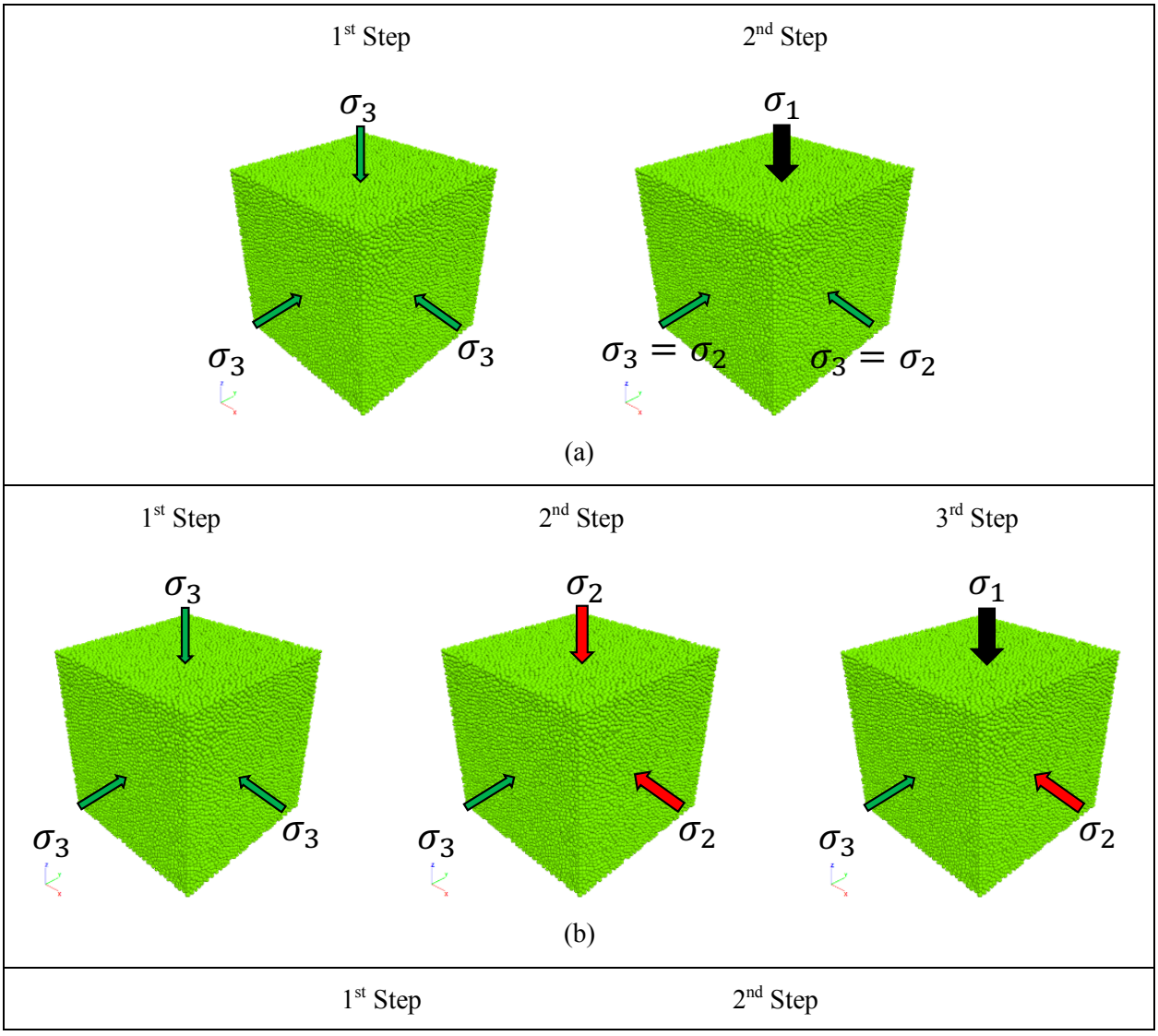

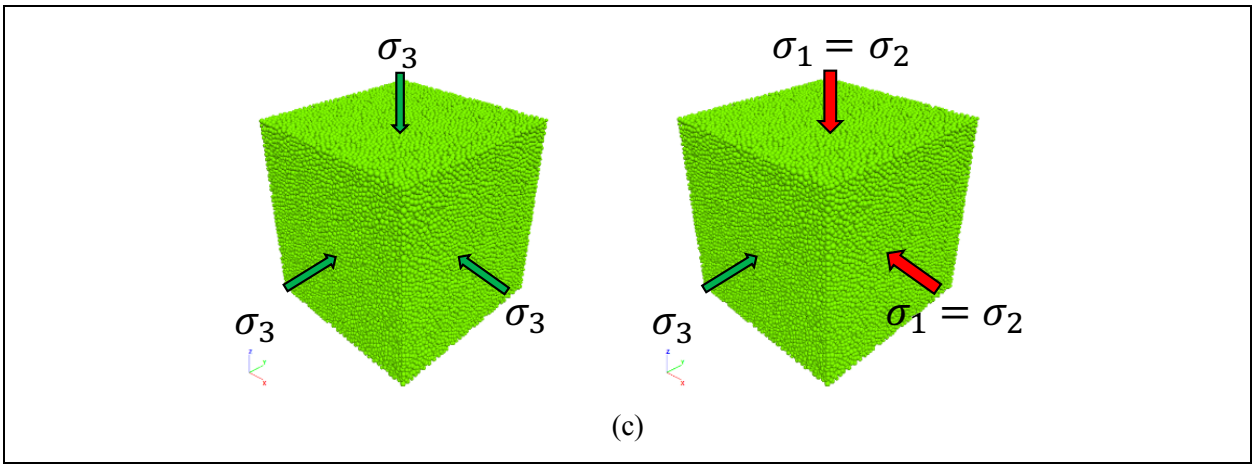

894 **Fig. 10** Different steps of applying the minor, intermediate and major principal stresses for the (a) triaxial
895 compression tests, (b) polyaxial compression tests and (c) biaxial compression tests.

896

897

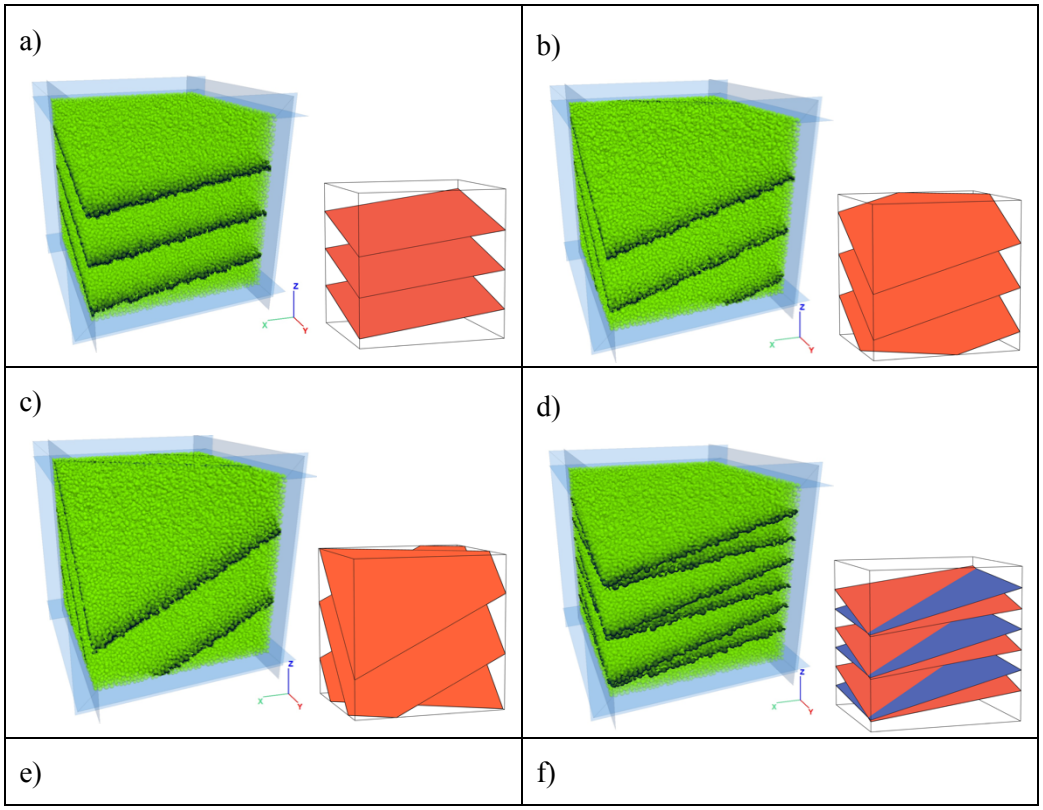

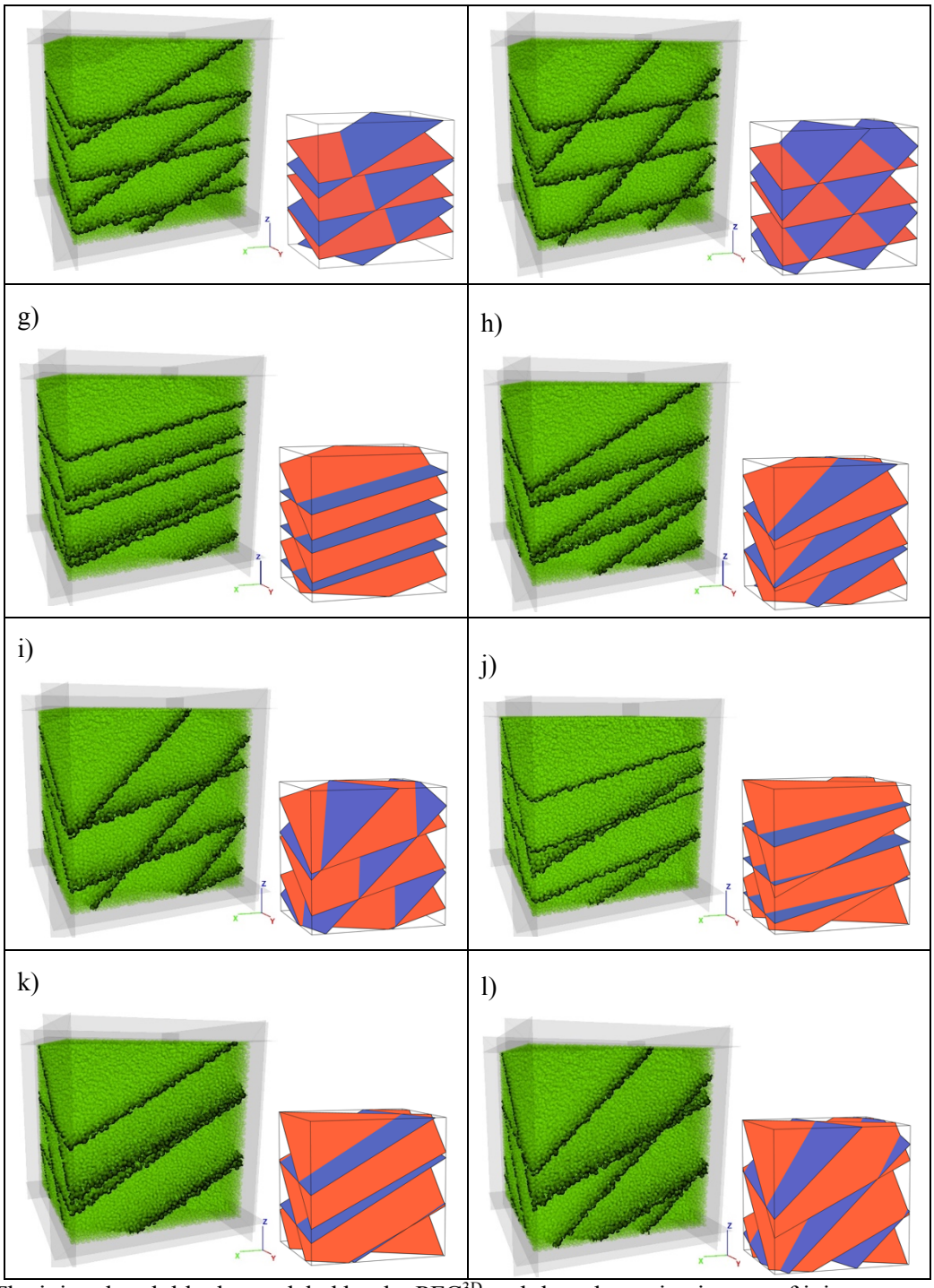

Fig. 11 The jointed rock blocks modeled by the PFC^{3D} and the schematic pictures of joint systems: (a), (b) and (c) have 3 joints with the dip direction of 30° and the dip angles of 15°, 30° and 45°, respectively; (d), (e) and (f) have 6 joints formed from 2 joint sets, 30° joint dip direction and 15° joint dip angle for the first joint set and 75° joint dip direction and the dip angles of 15°, 30° and 45° for the second joint set, respectively; (g), (h) and (i) have 6 joints formed from 2 joint sets, 30° joint dip direction and 30° joint dip angle for the first joint set and 75° joint dip direction and the dip angles of 15°, 30° and 45° for the second joint set, respectively; (j), (k) and (l) have 6 joints formed from 2 joint sets, 30° joint dip direction and 45°

joint dip angle for the first joint set and 75° joint dip direction and the dip angles of 15°, 30° and 45° for the second joint set, respectively; (In the schematic pictures, the blue planes are 1st joint set and red planes are 2nd joint set; the maximum principal stress, the intermediate principal stress and the minimum principal stresses are applied on the top face, on the front left face and on the right front face, respectively).

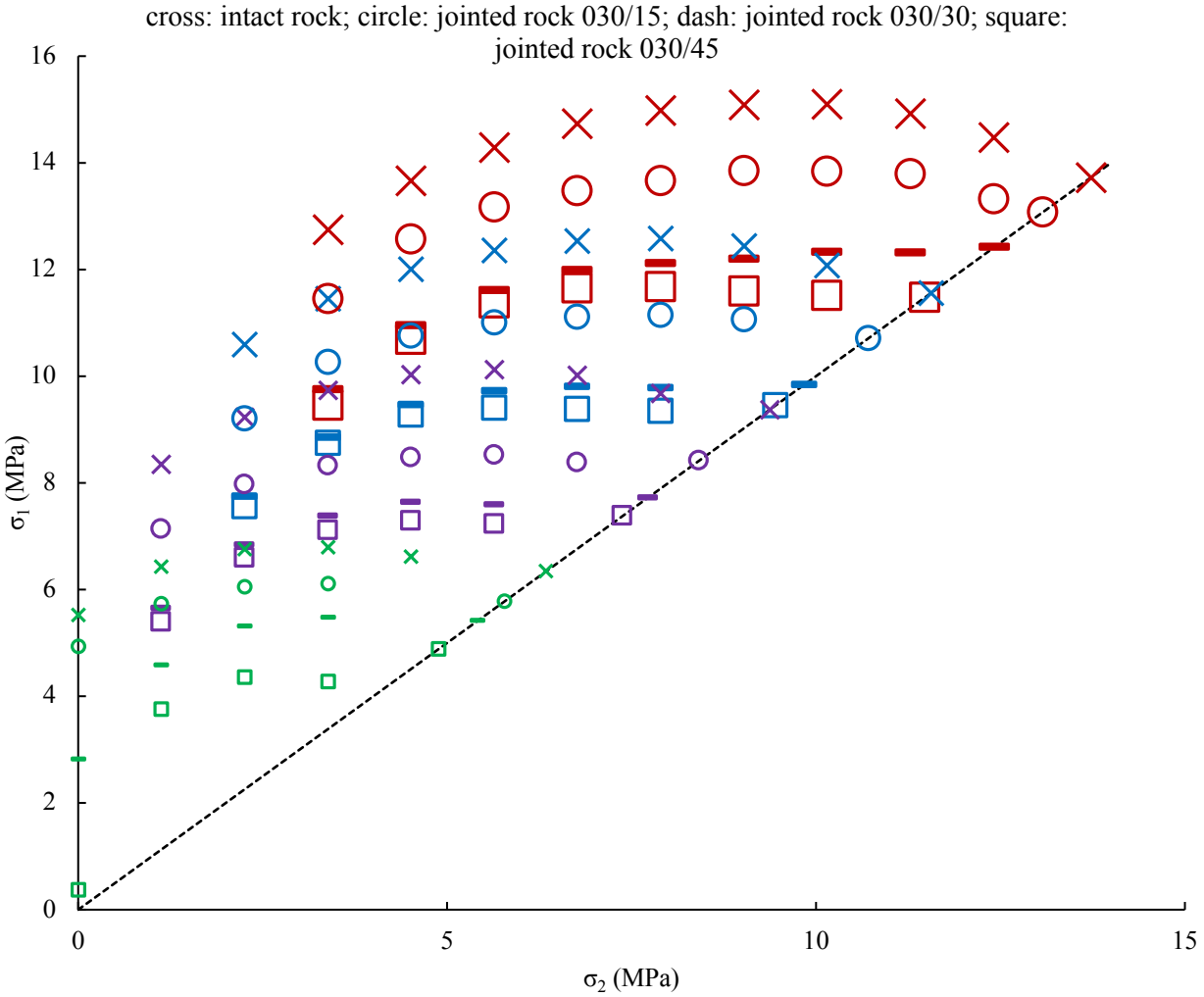

Fig. 12 Polyaxial test results obtained from PFC^{3D} modeling for the intact rock model and jointed rock models with one joint set having 3 joints with the dip direction of 30° and the various joint dip angles from 15° to 45° at an interval of 15°.

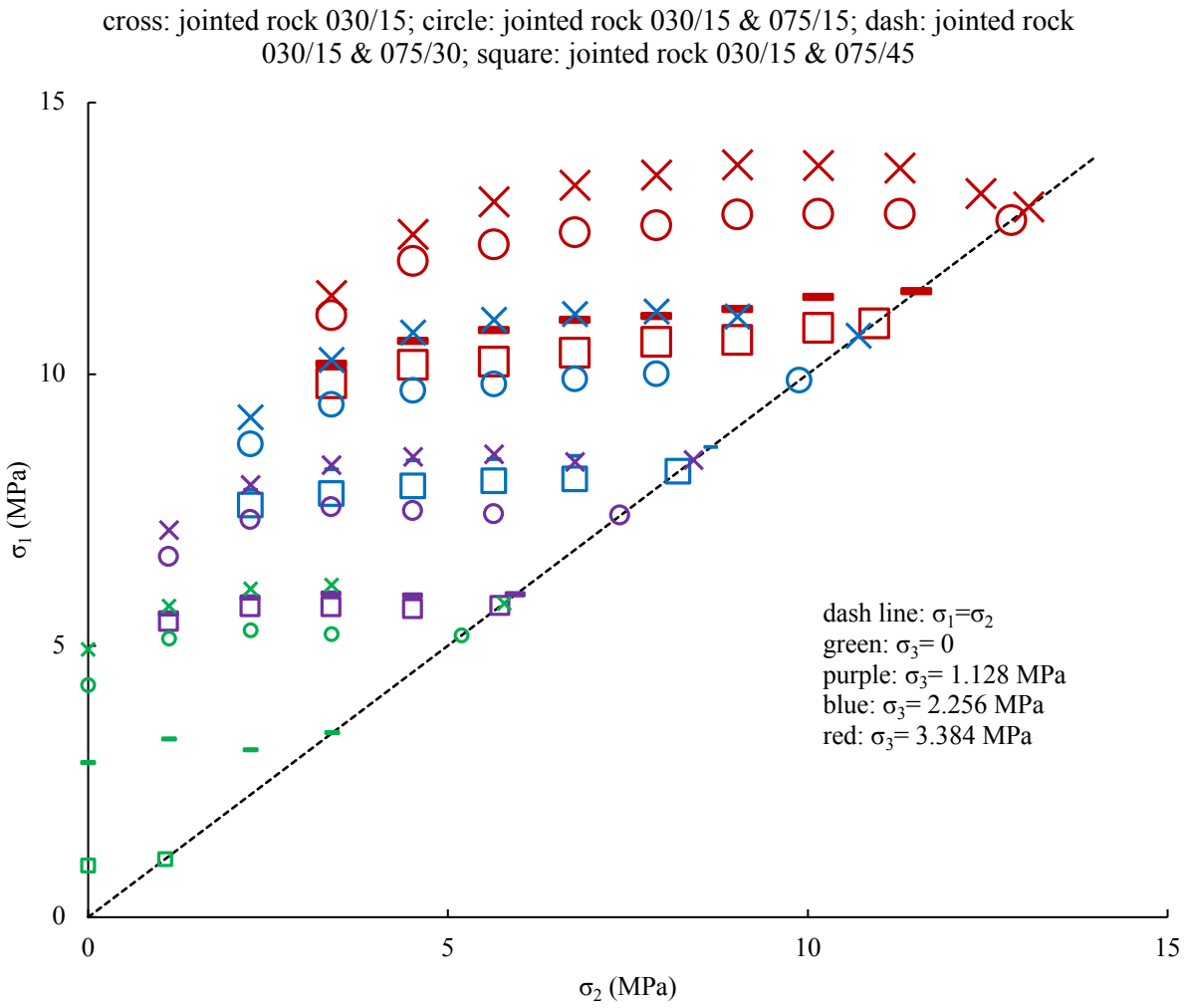

916

917 **Fig. 13** Polyaxial test results obtained from PFC^{3D} modeling for the jointed rock model having 3 joints with
918 30° joint dip direction and 15° joint dip angle and the jointed rock models having 6 joints formed from 2
919 joint sets with 30^{o} joint dip direction and 15° joint dip angle for the first joint set and 75° joint dip direction
920 and the various joint dip angles from 15° to 45° at an interval of 15° for the second joint set.

921

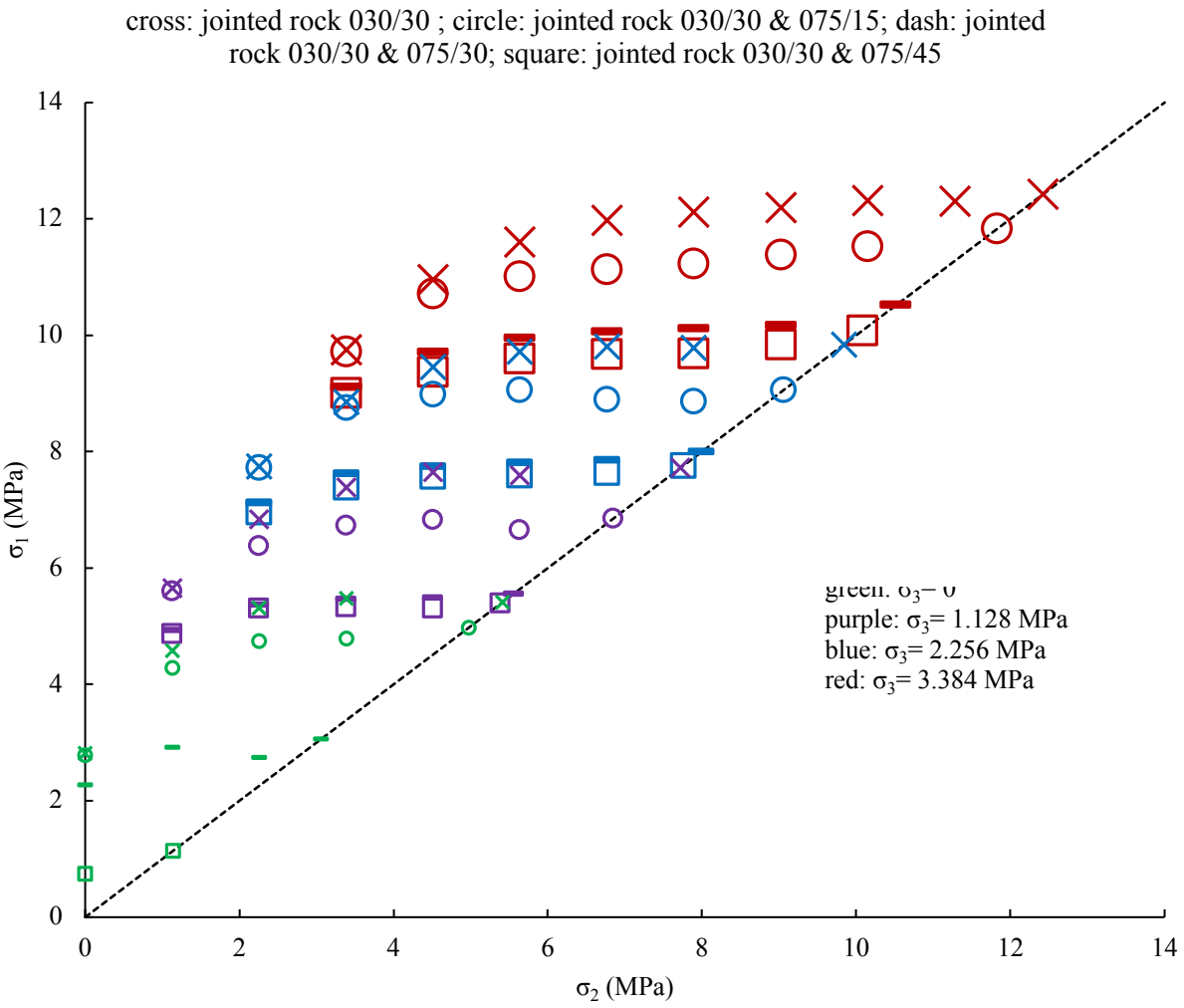

922

923 **Fig. 14** Polyaxial test results obtained from PFC^{3D} modeling for the jointed rock model having 3 joints with
924 30° joint dip direction and 30° joint dip angle and the jointed rock models having 6 joints formed from 2
925 joint sets with 30° joint dip direction and 30° joint dip angle for the first joint set and 75° joint dip direction
926 and the various joint dip angles from 15° to 45° at an interval of 15° for the second joint set.

927

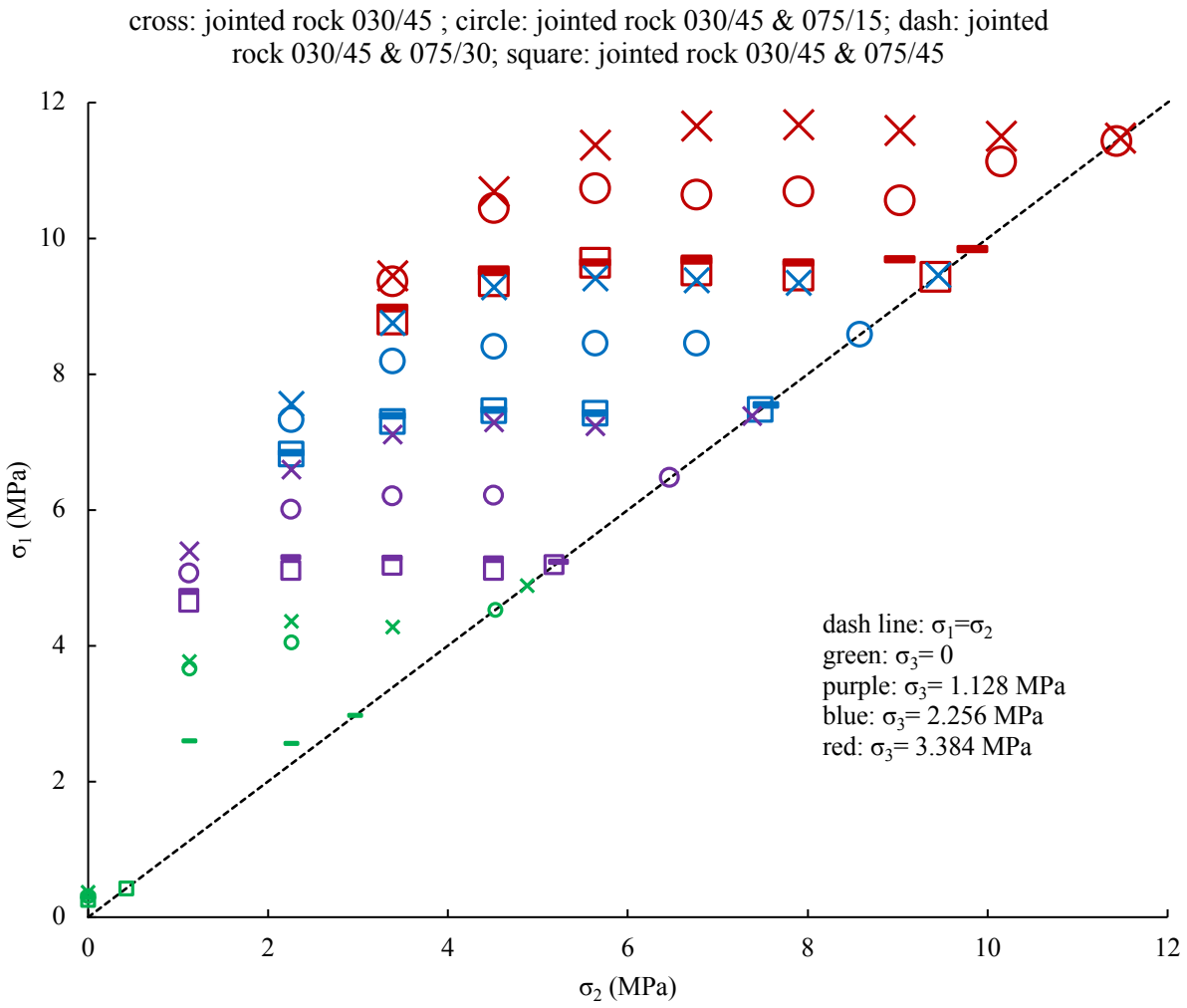

928

929 **Fig. 15** Polyaxial test results obtained from PFC^{3D} modeling for the jointed rock model having 3 joints with
930 30° joint dip direction and 45° joint dip angle and the jointed rock models having 6 joints formed from 2
931 joint sets with 30^{o} joint dip direction and 45° joint dip angle for the first joint set and 75° joint dip direction
932 and the various joint dip angles from 15° to 45° at an interval of 15° for the second joint set.

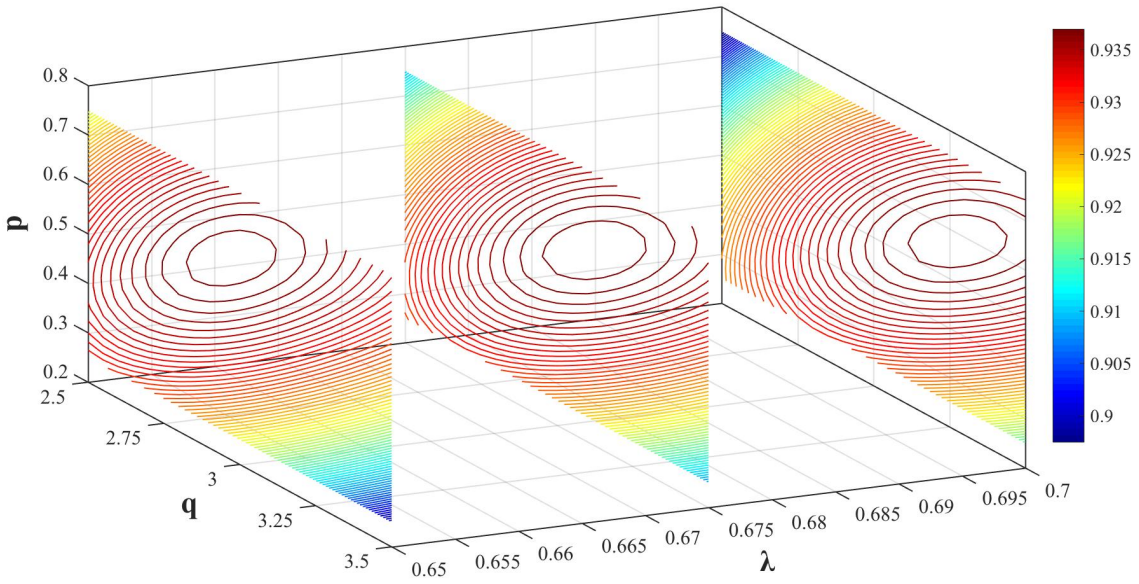

933

934

935 **Fig. 16** Obtained R^2 values of the new rock mass strength criterion using equation 13 for different
936 combinations of *p, q* on the cross-sectional planes of $\lambda = 0.65$, $\lambda = 0.675$ and $\lambda = 0.70$ (color bar shows the
937 R^2 values).

938

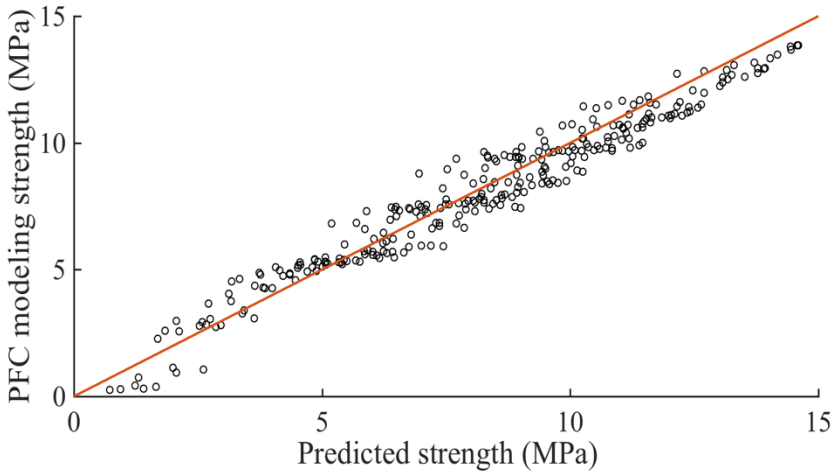

939

940 **Fig. 17** Predicted strength values based on the new rock mass strength criterion based on equation 13 versus
941 the strength values from PFC^{3D} modeling for all 284 data points from 12 different joint systems having
942 different boundary conditions ($R^2 = 0.94$)

943

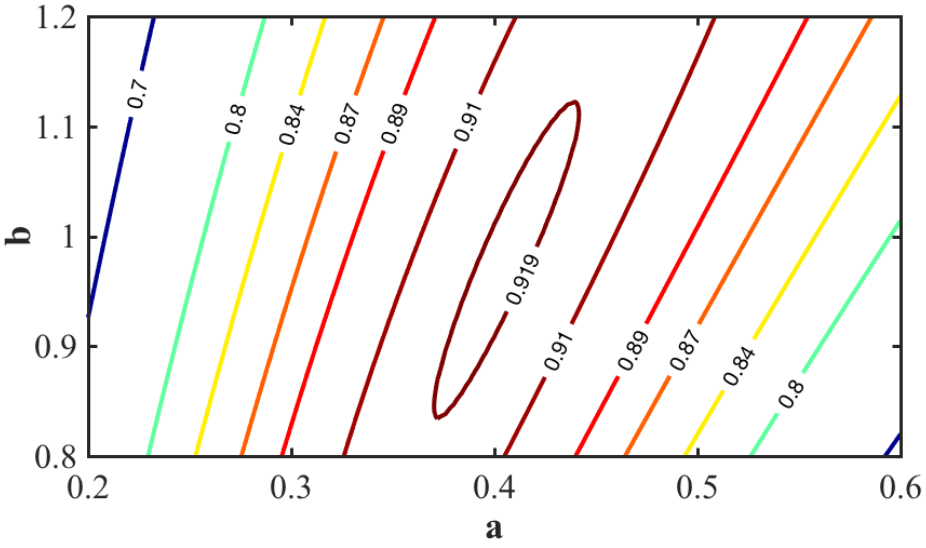

Fig. 18 Obtained R^2 values of the new rock mass strength criterion using equation 14 for different combinations of a and b

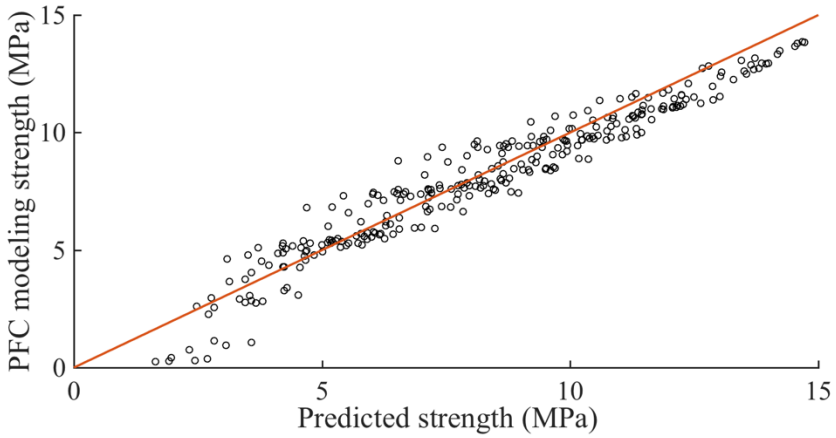

Fig. 19 predicted strength value based on the new rock mass strength criterion using equation 14 versus the strength value from PFC^{3D} for all 284 data points from 12 different joint systems and under different boundary conditions ($R^2 = 0.92$)

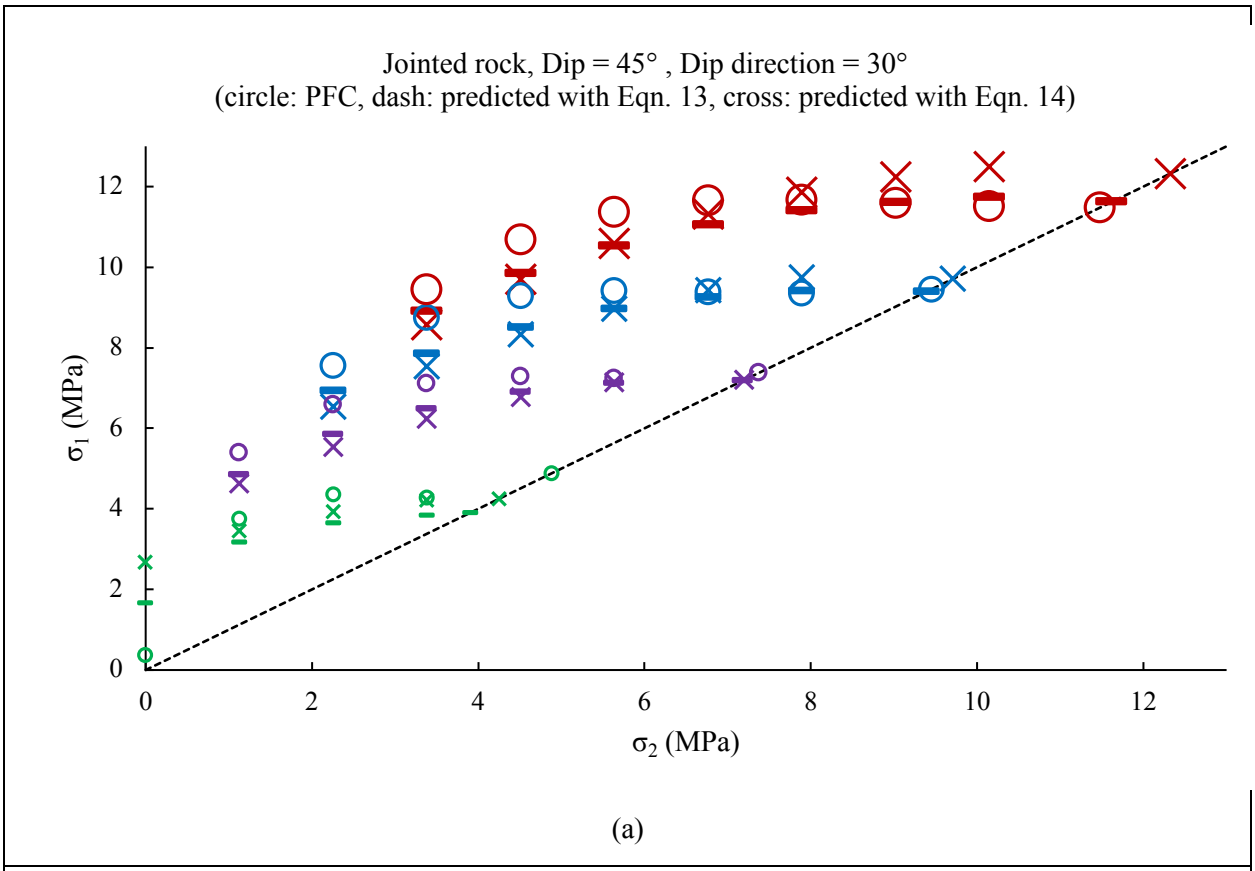
Jointed rock, Dip = 45° , Dip direction = 30°
(circle: PFC, dash: predicted with Eqn. 13, cross: predicted with Eqn. 14)
σ1 (MPa)
σ2 (MPa)
0
2
4
6
8
10
12

(a)

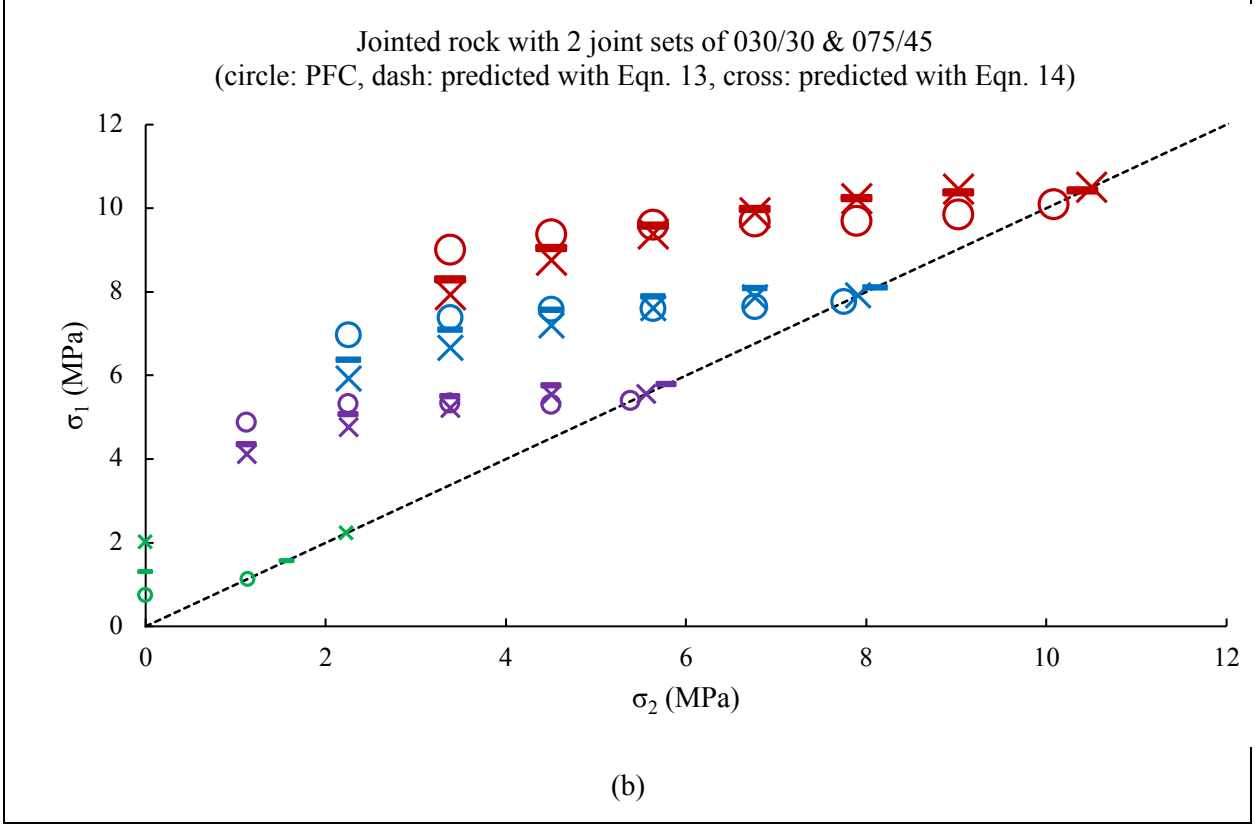
Jointed rock with 2 joint sets of 030/30 & 075/45
(circle: PFC, dash: predicted with Eqn. 13, cross: predicted with Eqn. 14)
σ1 (MPa)
σ2 (MPa)
0
2
4
6
8
10
12

(b)

Fig. 20 Comparison of the polyaxial strength results obtained from the PFC^{3D} modeling with that obtained from the new rock mass strength criteria based on Equations 13 and 14, respectively for the jointed rock block models (a) having 3 joints with dip angle and dip direction of 45° and 30°, respectively and (b) having 6 joints formed from 2 joint sets with 30° joint dip direction and 30° joint dip angle for the first joint set and 75° joint dip direction and 45° joint dip angle for the second joint set.

Table 1

Estimated macro mechanical property values for the synthetic rock from laboratory tests and PFC^{3D} modeling results

	Uniaxial strength (MPa)		Tensile strength (MPa)		Cohesion (MPa)	Angle of internal friction (deg.)	Young's modulus (GPa)		Poisson's ratio
Experimental tests	Range 5.28 - 6.09	Avg. 5.78	Range 1.03 - 1.57	Avg. 1.23	1.9	24	Range 0.99 - 1.21	Avg. 1.07	0.20
PFC^{3D} modeling	5.64		1.35		2.0	22	1.03		0.22

Table 2

Estimated macro mechanical property values for the synthetic rock joint from laboratory tests and PFC^{3D} modeling results

	Shear stiffness (GPa/m)		B (1/mm)		Joint friction angle (deg.)
Experimental tests	Range 0.4 - 0.9	Avg. 0.59	Range 19.8 – 36.8	Avg. 28.9	27.5
PFC^{3D} modeling	0.6		29		27

Table 3

Experimental and PFC^{3D} modeling results of the polyaxial and triaxial compression tests for the synthetic intact rock and the jointed rock blocks having 3 joints with the dip direction of 30° and joint dip angles of 15° or 30°

		sample	σ_3 (MPa)	σ_2 (MPa)	σ_1 (MPa) Experimental	σ_1 (MPa) PFC^{3D}
Intact rock		GB1	0	1.128	6.030	6.431
		GB2	0	2.256	6.642	6.763
Jointed rock (dip direction = 30°)	**Dip =15°**	GC15-1	1.128	3.384	8.301	8.325
		GC15-2	1.128	4.512	9.075	8.475
		GC15-3	2.256	2.256	9.165	9.200
		GC15-4	2.256	4.512	10.792	10.761
		GC15-5	2.256	7.896	10.856	11.151
		GC15-6	3.384	3.384	11.266	11.447
	Dip =30°	GC30-1	1.128	5.640	8.124	7.595
		GC30-2	2.256	2.256	8.304	7.742
		GC30-3	2.256	5.640	9.311	9.723
		GC30-4	2.256	7.896	9.578	9.779
		GC30-5	3.384	3.384	9.460	9.751

Table 4

Calibrated micro mechanical parameter values of the Linear Parallel Bond Model for the synthetic intact rock in PFC^{3D} (minimum particle diameter, D_{min}, maximum particle diameter, D_{max}, contact Young's modulus, E_c, bond Young's modulus, $\bar{E}_c$, contact friction coefficient, μ, bond tensile strength, $\bar{\sigma}_c$, bond shear strength, $\bar{\tau}_s$, the ratio of normal to shear stiffness for contact, k_r, ratio of normal to shear stiffness for bond, $\bar{k}_r$ and bond radius fraction, $\overline{\lambda)}$.

LPBM
$D_{min} = 2.7$ mm
$m_r = D_{Max}/D_{min} = 1.66$
E_c=$\bar{E}_c$=1.25 GPa
k_r=$\bar{k}_r$=2.5
μ=0.6
mean $\bar{\sigma}_c$= mean $\bar{\tau}_s$= 4.4 MPa
std. dev. $\bar{\sigma}_c$= std. dev. $\bar{\tau}_s$=1.1 MPa
$\bar{\lambda}$ =1

Table 5

Calibrated micro mechanical parameter values of the Modified Smooth Joint Contact Model for the synthetic rock joint in PFC^{3D} using the JSC approach

MSJCM
$\boldsymbol{\mu^J} = 0.5$
$\boldsymbol{k_s^J}(GPa/m) = 1.0$
$\boldsymbol{k_{n_{min}}^J}(GPa/m) = 4.0$
$\boldsymbol{B^J}(1/mm) = 31.0$

Table 6

The computed fracture tensor components in x, y, and z directions (the minimum, intermediate and maximum principal stress directions, respectively) for 12 joint systems of the jointed rock blocks.

Joint system (Dip direction/Dip)	**F_{xx} (F_{33})**	**F_{yy} (F_{22})**	**F_{zz} (F_{11})**	**F_{xy} (F_{32})**	**F_{xz} (F_{31})**	**F_{yz} (F_{21})**
030/15	0.060	0.179	3.326	0.103	0.446	0.772
030/30	0.230	0.690	2.759	0.398	0.796	1.380
030/45	0.446	1.337	1.783	0.772	0.891	1.544
030/15 & 075/15	0.282	0.195	6.653	0.163	1.307	1.003
030/15 & 075/30	0.840	0.235	5.835	0.312	1.845	1.147
030/15 & 075/45	1.199	0.261	4.547	0.409	1.625	1.088
030/30 & 075/15	0.453	0.706	6.086	0.458	1.657	1.610
030/30 & 075/30	1.010	0.746	5.268	0.607	2.196	1.755
030/30 & 075/45	1.369	0.722	3.980	0.703	1.976	1.696
030/45 & 075/15	0.669	1.353	5.109	0.832	1.752	1.775
030/45 & 075/30	1.226	1.393	4.292	0.981	2.291	1.919
030/45 & 075/45	1.585	1.419	3.004	1.077	2.070	1.860